Cell

Essential Regulation of Cell Bioenergetics by Constitutive $InsP_3$ Receptor Ca^{2+} Transfer to Mitochondria

César Cárdenas,[1] Russell A. Miller,[3] Ian Smith,[5] Thi Bui,[4] Jordi Molgó,[6] Marioly Müller,[1] Horia Vais,[1] King-Ho Cheung,[1] Jun Yang,[1] Ian Parker,[5] Craig B. Thompson,[4] Morris J. Birnbaum,[3] Kenneth R. Hallows,[7] and J. Kevin Foskett[1,2,*]
[1]Department of Physiology
[2]Department of Cell and Developmental Biology
[3]Institute for Diabetes, Obesity and Metabolism
[4]Abramson Cancer Institute and Department of Cancer Biology
University of Pennsylvania, Philadelphia, PA 19104, USA
[5]Department of Neurobiology and Behavior, University of California, Irvine, CA 92697, USA
[6]CNRS, Institute de Neurobiologie Alfred Fessard, FRC2118, Laboratoire de Neurobiologie Cellulaire et Développement, UPR 3294, 91198 Gif-sur-Yvette Cedex, France
[7]Department of Medicine, University of Pittsburgh, Pittsburgh, PA 15261, USA
*Correspondence: foskett@mail.med.upenn.edu
DOI 10.1016/j.cell.2010.06.007

SUMMARY

Mechanisms that regulate cellular metabolism are a fundamental requirement of all cells. Most eukaryotic cells rely on aerobic mitochondrial metabolism to generate ATP. Nevertheless, regulation of mitochondrial activity is incompletely understood. Here we identified an unexpected and essential role for constitutive $InsP_3R$-mediated Ca^{2+} release in maintaining cellular bioenergetics. Macroautophagy provides eukaryotes with an adaptive response to nutrient deprivation that prolongs survival. Constitutive $InsP_3R$ Ca^{2+} signaling is required for macroautophagy suppression in cells in nutrient-replete media. In its absence, cells become metabolically compromised due to diminished mitochondrial Ca^{2+} uptake. Mitochondrial uptake of $InsP_3R$-released Ca^{2+} is fundamentally required to provide optimal bioenergetics by providing sufficient reducing equivalents to support oxidative phosphorylation. Absence of this Ca^{2+} transfer results in enhanced phosphorylation of pyruvate dehydrogenase and activation of AMPK, which activates prosurvival macroautophagy. Thus, constitutive $InsP_3R$ Ca^{2+} release to mitochondria is an essential cellular process that is required for efficient mitochondrial respiration and maintenance of normal cell bioenergetics.

INTRODUCTION

Metabolism provides energy in a useful form to maintain homeostasis and perform work in all cells. Adenosine-5′-triphosphate (ATP) production from substrate oxidation and the release of free energy from its hydrolysis must be balanced and sufficient to support cell metabolic needs, including growth, proliferation, production of metabolites, and maintenance of homeostatic processes. Most eukaryotic cells rely on mitochondrial oxidative phosphorylation as the major source of ATP. However, the mechanisms by which mitochondrial respiration and ATP synthesis are controlled in intact cells are still not completely understood. Respiratory control models involving kinetic feedback from the products of ATP hydrolysis, allosteric effects of ATP and inorganic phosphate (P_i), rates of reducing equivalent delivery to mitochondria, O_2 availability, and various controls over respiratory chain components are involved (Balaban, 1990; Brown, 1992; Huttemann et al., 2008). Nevertheless, neither the factors that exert primary control of oxidative phosphorylation and ATP production in the intact cell nor the signal transduction mechanisms that support the steady-state balance of ATP production and utilization are well understood (Balaban, 1990).

Normal respiration can be altered in several pathological situations (Smeitink et al., 2006; Wallace, 2005), including cancer (Vander Heiden et al., 2009), insufficient nutrient availability, ischemia, injury and exposure to metabolic inhibitors (Huttemann et al., 2008), neurodegenerative (Mattson et al., 2008) and cardiovascular (Gustafsson and Gottlieb, 2008) diseases, and aging (Balaban et al., 2005). In response to decreased cellular ATP, cells employ a variety of pathways to restore homeostasis, including activation of AMP-activated protein kinase (AMPK) (Hardie, 2007). AMPK phosphorylates substrates to limit anabolic pathways that consume ATP and to activate catabolic pathways to generate substrates to support oxidative phosphorylation (Hardie, 2007). Another mechanism involves activation of macroautophagy (autophagy), a degradation pathway involving delivery of cytoplasmic constituents by double-membrane autophagosomes (AV) that fuse with lysosomal membranes (Klionsky, 2007). Under metabolic stress, prosurvival autophagy is induced, promoting recycling

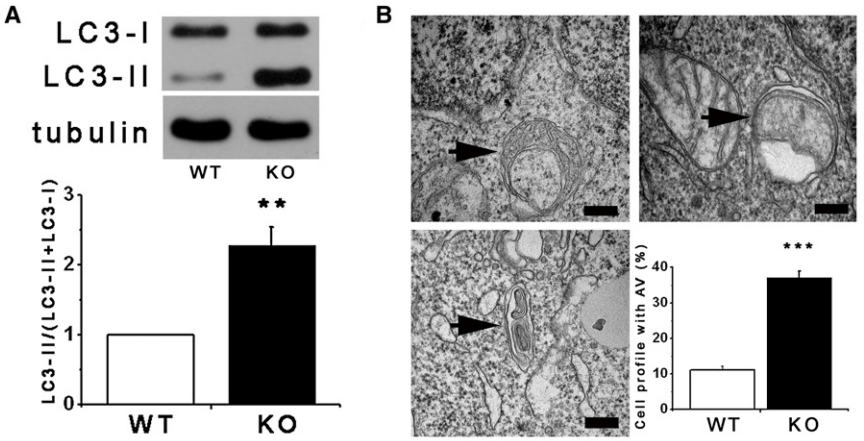

Figure 1. $InsP_3R$-Deficient Cells Have Elevated Autophagy in Nutrient-Rich Conditions

(A) Western blot of LC3 or tubulin in DT40-WT and DT40-KO cells (top) and quantification of LC3-II/(LC3-I + LC3-II) (bottom) expressed as fold increase over WT levels (n = 8).

(B) TEM of DT40-KO cells showing autophagosomes (AV, arrows) and summary of cell profiles containing AV. Four hundred profiles counted in four experiments. Bars, 50 nm.

(C) Confocal images of GFP-LC3 in DT40-WT and DT40-KO cells (left and middle panels). Arrows show LC3 puncta (900 cells from three experiments with 15 random fields/experiment). ***$p < 0.001$, **$p < 0.01$; Bar, 10 μm.

See also Figure S1.

of metabolites to meet metabolic demands, through synthesis of new macromolecules or by their oxidation in mitochondria to maintain ATP levels (Levine and Kroemer, 2008; Lum et al., 2005). Autophagy also functions in developmental cell death, tumor suppression, immunity, and aging, and it has been implicated in neurodegeneration, cardiovascular disease, and cancer (Levine and Kroemer, 2008).

Here, we have identified a fundamental cellular metabolic control mechanism involving activity of the endoplasmic reticulum-localized inositol trisphosphate receptor ($InsP_3R$) Ca^{2+} release channel. In the absence of basal constitutive low-level Ca^{2+} signaling by the $InsP_3R$, cells become metabolically compromised as a result of diminished Ca^{2+} uptake by mitochondria. Constitutive mitochondrial Ca^{2+} uptake of $InsP_3R$-released Ca^{2+} is fundamentally required to maintain sufficient mitochondrial NADH production to support oxidative phosphorylation in resting cells. Absence of this Ca^{2+} transfer results in inhibition of pyruvate dehydrogenase and activation of AMPK, which activates prosurvival autophagy by an mTOR-independent mechanism. These results reveal a heretofore unexpected and fundamentally essential role for constitutive low-level $InsP_3R$ Ca^{2+} release to mitochondria to maintain viable levels of oxidative phosphorylation.

RESULTS

The $InsP_3R$ Is Required to Inhibit Constitutive Autophagy in Normal Conditions

Chicken DT40 B lymphocytes with all three $InsP_3R$ isoforms genetically deleted (DT40-KO) is a uniquely $InsP_3R$ null cell line (Sugawara et al., 1997). Despite lack of $InsP_3R$, DT40-KO cells proliferate indefinitely in normal culture conditions. Transmission electron microscopy (TEM) revealed a significantly high percentage of knockout (KO) cells with autophagosomes (AV) (36% ± 2%) compared with $InsP_3R$-expressing wild-type (WT) cells (11% ± 1%; Figure 1B). Elevated autophagy in KO cells in normal growth conditions was also detected by quantitative measurements of the autophagy marker LC3-II (Klionsky et al., 2008) (Figure 1A). In addition, presence of LC3-GFP puncta associated with early AV formation (Klionsky et al., 2008) was higher in KO (18% ± 4%) versus WT (5% ± 1%) cells (Figure 1C). These results suggest that absence of $InsP_3R$ in DT40-KO cells increases constitutive levels of autophagy. Autophagy was not previously observed in DT40-KO cells (Vicencio et al., 2009), but knockdown of $InsP_3R$ or its pharmacological inhibition also induces autophagy (Criollo et al., 2007 and below).

Autophagy in KO cells was not associated with induction of the unfolded protein response (not shown). Lower level of autophagy observed in $InsP_3R$-expressing WT cells was not due to intrinsic defects in autophagy, as serum starvation or leucine deprivation induced comparable autophagy in WT and KO cells (Figures S1A–S1D available online). Furthermore, mTOR inhibition by rapamycin strongly increased LC3-II levels, whereas 3-methyladenine (3MA), an inhibitor of class III phosphoinositide 3-kinase (PI-3 kinase) involved in AV formation

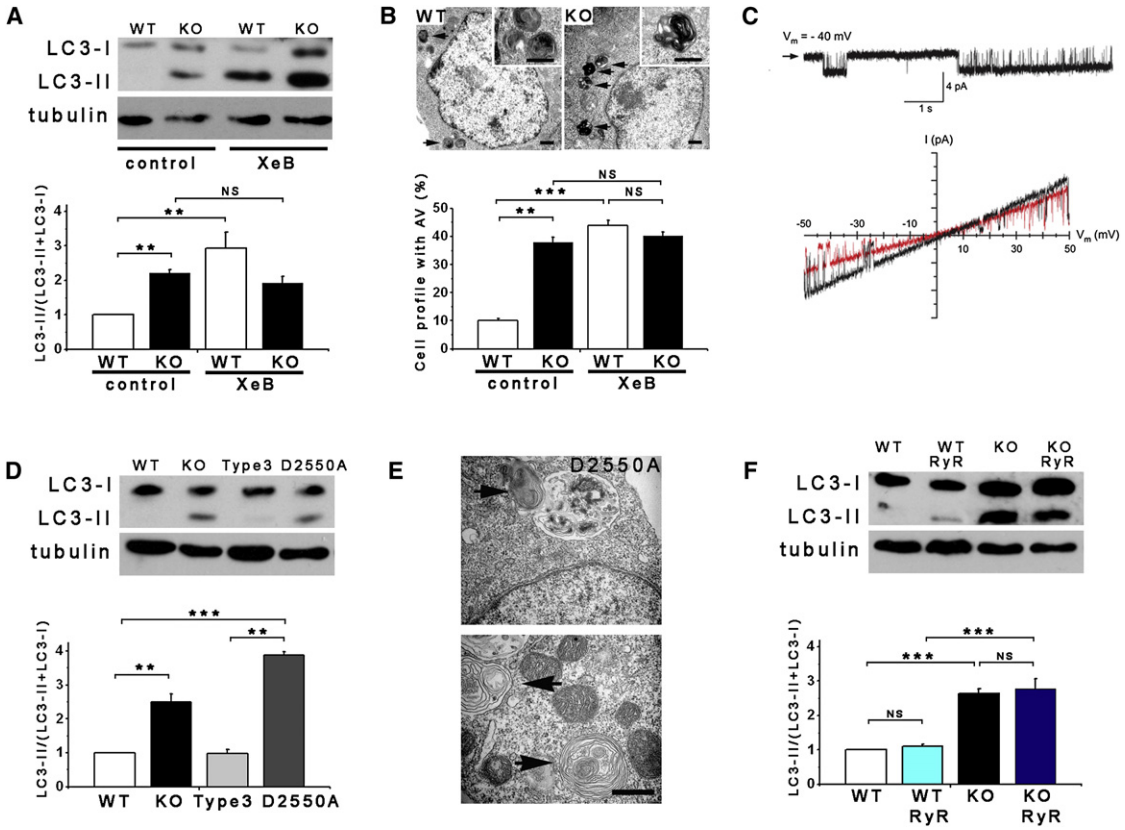

Figure 2. $InsP_3R$ Dependence of Autophagy Suppression in Nutrient-Rich Conditions

(A) XeB (2 μM for 1 hr) induces autophagy in DT40-WT cells to levels observed in DT40-KO cells (n = 6).

(B) TEM of WT (left) and KO (right) cells showing AV (arrows and insets) after 1 hr incubation with 2 μM XeB. Bars, 500 nm. Bottom panel: Summary of 100 cells per experiment counted from 15 fields (n = 3).

(C) Current recordings in isolated nuclei from DT40-KO cells expressing D2550A-$InsP_3R$-3. Upper: Typical gating; arrow represents closed channel current level. Bottom: Currents during voltage ramps in control solution (black) and in presence of 10 mM lumenal Ca^{2+} (red). Lack of normal shift in reversal potential indicates absence of Ca^{2+} permeability.

(D) Expression of $InsP_3R$-3, but not Ca^{2+}-impermeable D2550A-$InsP_3R$-3, suppresses autophagy in KO cells (n = 3).

(E) TEM of AV (arrows) in cells stably transfected with D2550A-$InsP_3R$-3. Bar = 500 nm.

(F) RyR-2 expression fails to suppress autophagy in KO cells (n = 3).

***p < 0.001; **p < 0.01; NS, not significant. See also Figure S2, Figure S3, and Figure S4.

(Levine and Kroemer, 2008), inhibited LC3-II formation in both lines (Figure S1E). Inhibition of lysosomal proteases enhanced LC3-II in both lines, especially in KO cells (Figures S1F and S1G), indicating that elevated autophagy in KO cells is due primarily to enhanced AV formation.

The specific $InsP_3R$ inhibitor xestospongin B (XeB) (Jaimovich et al., 2005) increased LC3-II only in WT cells (Figure 2A). XeB increased AV by 22% ± 1% (LC3-GFP puncta; Figure S2A) to 42% ± 2% (TEM; Figure 2B) in WT cells, whereas KO cells were unaffected. Reduction of $InsP_3$ production by inhibition of phospholipase C (PLC, by 5 μM U73122) or inositol monophosphatase (IMPase, by 50 μM L-690,488) strongly enhanced LC3-II in WT cells, whereas it was without effect on autophagy already present in KO cells (Figures S2B and S2C). XeB also strongly enhanced LC3-II levels and puncta in primary rat pulmonary smooth muscle cells and hepatocytes, and the human breast cancer cell line MCF-7 (Figures S3A–S3C, S3G, and S3H), indicating that autophagy suppression by $InsP_3R$ activity is a general phenomenon operative in many cell types.

Functional $InsP_3R$ Restores Nutrient-Dependent Suppression of Autophagy in KO Cells

Stable expression of $InsP_3R$-3 (Figure S2D) completely rescued elevated autophagy in KO cells, measured as either LC3-II content (Figure 2D and Figure S2E) or AV visualization (not shown). To determine if its Ca^{2+} channel function was required, we examined cells expressing $InsP_3R$-3 containing Thr at position 2591 replaced with Ala (T2591A). T2591A-$InsP_3R$-3 expresses at normal levels (Figure S2D) but lacks ion channel activity as a result of a defective channel gate (J.K.F., unpublished data). In contrast to $InsP_3R$-3, T2591A-$InsP_3R$-3 did not suppress constitutive autophagy (Figure S2E). To determine whether failure to rescue was due specifically to loss of Ca^{2+} release activity, we examined KO cells expressing

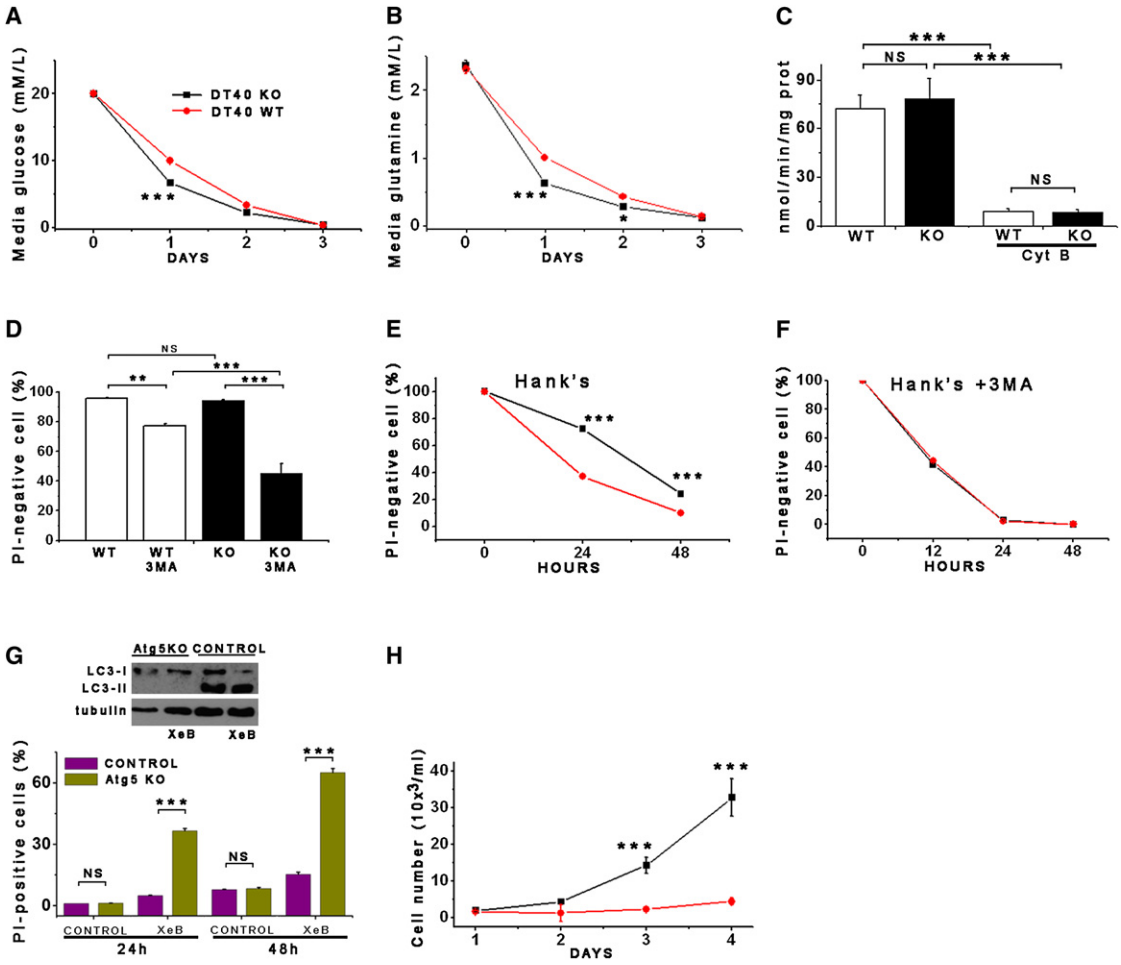

Figure 3. Lack of $InsP_3R$ Ca^{2+} Release Activity Activates Prosurvival Mechanisms

(A and B) Glucose (A) and glutamine (B) consumption measured daily in DT40 cells.

(C) Cytochalasin B (Cyt B)-sensitive deoxyglucose uptake by WT and KO cells (n = 3).

(D) Effects of autophagy inhibition by 3MA in nutrient-rich media on viability (PI-negative cells) of WT and KO cells after 24 hr (n = 3).

(E and F) Survival of WT and KO cells in starvation conditions (Hank's) in absence (E) and presence (F) of 3MA (n = 3).

(G) Death (PI-positive cells) of Atg5-deficient primary hepatocytes induced by XeB (n = 3).

(H) Recovery of WT and KO cells after 24 hr starvation. Same number of cells seeded in complete medium (n = 3).

Error bars shown when bigger than points. ***p < 0.001, **p < 0.01.

D2550A-$InsP_3R$-3 (Figure S2D). This mutant gates normally, whereas it has complete loss of Ca^{2+} permeability (Figure 2C). D2550A-$InsP_3R$-3 failed to suppress constitutive autophagy, with a tendency in these cells to have enhanced levels (Figures 2D and 2E). D2550A- and WT-$InsP_3R$-3 bound similarly to Beclin-1 (Figure S2K), indicating that disruption of Beclin-1 binding (Vicencio et al., 2009) does not account for autophagy induction by $InsP_3R$ inhibition. Rather, these results demonstrate that the Ca^{2+} release activity of $InsP_3R$ is necessary for autophagy suppression.

DT40-WT and DT40-KO cells were stably transfected with the type 2 ryanodine receptor (RyR2), an $InsP_3R$-related Ca^{2+} channel expressed in cardiac myocytes, brain neurons, and elsewhere (Fill and Copello, 2002). Caffeine triggered Ca^{2+} release (Figure S2F) whereas nontransfected cells failed to respond (not shown). Nevertheless, RyR2 expression was without effect on constitutive autophagy in KO cells (Figure 2F and Figure S2G). Thus, Ca^{2+} release specifically through $InsP_3R$ regulates autophagy in normal nutrient-rich conditions.

Requirement for $InsP_3R$ Ca^{2+} Signaling for Autophagy Suppression Is Not due to Ca^{2+} Dependence of Nutrient Uptake

Autophagy can be activated by insufficient nutrient uptake (Nicklin et al., 2009). DT40-KO cells reduced glucose in the medium by 67% (20 ± 0.2 to 6.6 ± 0.3 mM/l) in 24 hr, whereas WT cells decreased it by 50% (20 ± 0.02 to 10 ± 0.01 mM/l) (Figure 3A). Similarly, KO cells reduced glutamine by 75% (2.37 ± 0.07 to 0.6 ± 0.01 mM/l), whereas WT cells reduced it by 56% (2.31 ± 0.05 to 1 ± 0.07 mM/l) (Figure 3B). WT and KO cells had similar rates of cytochalasin-B-sensitive deoxyglucose

uptake (Figure 3C). Thus, autophagy activation in the absence of $InsP_3R$ is not caused by diminished nutrient uptake.

Autophagy Activated by Lack of $InsP_3R$ Activity Is a Cell Survival Mechanism

Viability was similar in KO (90.3% ± 1.7%) and WT (92.1% ± 2%) cells (Figure 3D), suggesting that autophagy in KO cells was not accelerating cell death. To evaluate a role in survival, autophagy was inhibited by pharmacological and genetic means. 3MA reduced viability of KO cells (48.3% ± 7% viable), whereas it had significantly less effect on WT cells (78.2% ± 2.1%; $p < 0.001$; Figure 3D). Effects on WT cell viability are consistent with an important housekeeping function of low-level basal autophagy (Levine and Kroemer, 2008). Treatment with XeB (5 μM for 24 hr) killed 38% ± 3% of autophagy-deficient primary hepatocytes from *Atg5* knockout mice compared with 1% ± 0.7% of littermate control cells (Figure 3G). At 48 hr, 65% ± 2.5% of the Atg5-deficient cells died, compared with 17% ± 0.8% of control cells. These results indicate that enhanced autophagy provides a survival mechanism. Consistent with this, when cells were subjected to acute nutrient deprivation by incubation in Hank's medium (24 hr), DT40-KO cells were resistant to death (78.2% ± 2.2% survival) compared with WT cells (36.2% ± 6% survival) (Figure 3E), and this difference was suppressed by 3MA (Figure 3F). When both lines were returned to normal growth medium after 24 hr in Hank's, KO cells recovered more rapidly than WT cells (Figure 3H). Thus, autophagy is activated in $InsP_3R$-KO cells as a prosurvival mechanism, and its chronic activation enables them to respond more rapidly and efficiently to nutrient stress, promoting their tolerance and rapid recovery when conditions improve.

AMPK Activity Is Enhanced by Absence of $InsP_3R$ Activity

Autophagy is activated as a survival mechanism in response to metabolic stress associated with insufficient growth factor stimulation or nutrient availability (Lum et al., 2005). An important mediator of this response is AMPK, a critical metabolic sensor (Hardie, 2007). Although DT40-KO cells do not lack growth factors or nutrients, they nevertheless display enhanced or similar nutrient uptake at the same time they depend on autophagy as a survival mechanism. We therefore examined the role of AMPK by quantifying phosphorylation of the catalytic α subunit as a marker for AMPK activity. Notably, KO cells had constitutively phosphorylated AMPK (P-AMPK) nearly 2-fold greater than in WT cells (Figure 4A). In agreement, phosphorylation of acetyl CoA carboxylase, an AMPK substrate, was also increased in KO cells (data not shown). Enhanced AMPK activity was caused by lack of $InsP_3R$ because XeB, U73122, or L-690,488 elevated P-AMPK in WT cells, notably to the same levels as in KO cells (Figure 4B, Figures S2H and S2I). Enhanced P-AMPK by XeB was also observed in primary smooth muscle cells and hepatocytes as well as in MCF-7 cells (Figures S3D–S3F). Importantly, treatment of hepatocytes with XeB increased AMP levels and the AMP:ATP ratio (Figure 4J). Elevated P-AMPK in KO cells was reduced to WT levels by expression of $InsP_3R$-3, but not by expression of Ca^{2+}-impermeable D2550A-$InsP_3R$-3 (Figure 4C) or RyR-2 (Figure 4D). Thus, both prosurvival autophagy and AMPK activity are upregulated by absence of $InsP_3R$ Ca^{2+} release activity.

AMPK, but Not mTOR, Is Required for Enhanced Autophagy Induced by Absence of $InsP_3R$ Activity

Enhanced AMPK activity can induce autophagy by inhibition of mTOR (Kimball, 2006). Nevertheless, mTOR phosphorylation was similar in DT40-KO and DT40-WT cells (Figure 4E). Furthermore, XeB did not affect P-mTOR in WT cells (Figure 4E), in contrast to its effects on autophagy and P-AMPK. Similarly, phosphorylation of 4E-BP1 or $p70^{S6K}$, two mTOR substrates, was similar in KO and WT cells and unchanged in WT cells exposed to XeB (Figures 4F and 4G). In contrast, P-$p70^{S6K}$ was reduced by starvation or rapamycin (Figure S2J), confirming that mTOR activity is normal in these cells. Thus, autophagy induced by lack of $InsP_3R$ activity correlates with enhanced AMPK activity, but the mTOR pathway does not appear to be involved.

To determine if AMPK nevertheless links lack of $InsP_3R$ Ca^{2+} release to autophagy activation, we employed pharmacological and genetic approaches. Treatment with the AMPK inhibitor compound C reduced P-AMPK (Figure 4I) and LC3-II (Figure 4H) in KO cells. This suggests that AMPK acts upstream and is required for autophagy activation in response to loss of $InsP_3R$ activity. To confirm this, we used HEK293 cells stably expressing either a doxycycline (DOX)-inducible dominant-negative α1-AMPK (HEK-K45R), WT α1-AMPK (HEK-WT), or the empty vector (HEK-EV) (Hallows et al., 2009; Bhalla et al., 2006). Control experiments confirmed that results obtained in the other cell types were recapitulated in HEK cells. Thus, XeB or U73122 each increased P-AMPK (Figure 5B and Figure S4A) and autophagy (Figure 5C, Figures S3I and S3J, and Figure S4B) as a result of enhanced autophagic flux (Figure S4C). IMPase inhibitors L-690-488 and L-690-330 also induced P-AMPK and autophagy, with L-690-488, with better cell penetration, having stronger effects (Figures S4D and S4E). P-$p70^{S6K}$ was unaffected by XeB (Figures S4G and S4J), indicating that XeB-induced autophagy in HEK cells was mTOR independent. Leucine deprivation, which induces autophagy by depressing mTOR activity (Meijer, 2008), potentiated effects of XeB (Figure S4H), and XeB was without effect on normal mTOR inhibition by Hank's or rapamycin (Figure S4G), consistent with additivity of mTOR-dependent and $InsP_3R$-associated-independent mechanisms. Thus, $InsP_3R$ Ca^{2+} release channel activity is required for mTOR-independent suppression of autophagy in HEK cells.

Overexpression of AMPK in HEK-WT cells (Figure 5A) increased P-AMPK (Figure 5B and Figure S4A) and enhanced LC3-II (Figure 5C, Figures S3I and S3J, and Figure S4B). XeB or U73122 induced autophagy and increased P-AMPK in control HEK-EV cells and HEK-WT cells, whereas neither compound induced autophagy or P-AMPK in HEK-K45R cells expressing dominant-negative AMPK (Figures 5B and 5C, Figures S3I and S3J, and Figures S4A and S4B). These results strongly link autophagy induced by loss of $InsP_3R$ activity to AMPK activation. In agreement, transient siRNA (Figure 5D) or stable DOX-inducible shRNA (Figure 5G) α1-AMPK knockdown blocked XeB-induced autophagy (Figures 5E and 5H and Figures S3I and S3J) and P-AMPK (Figures 5F and 5I). Together, these results

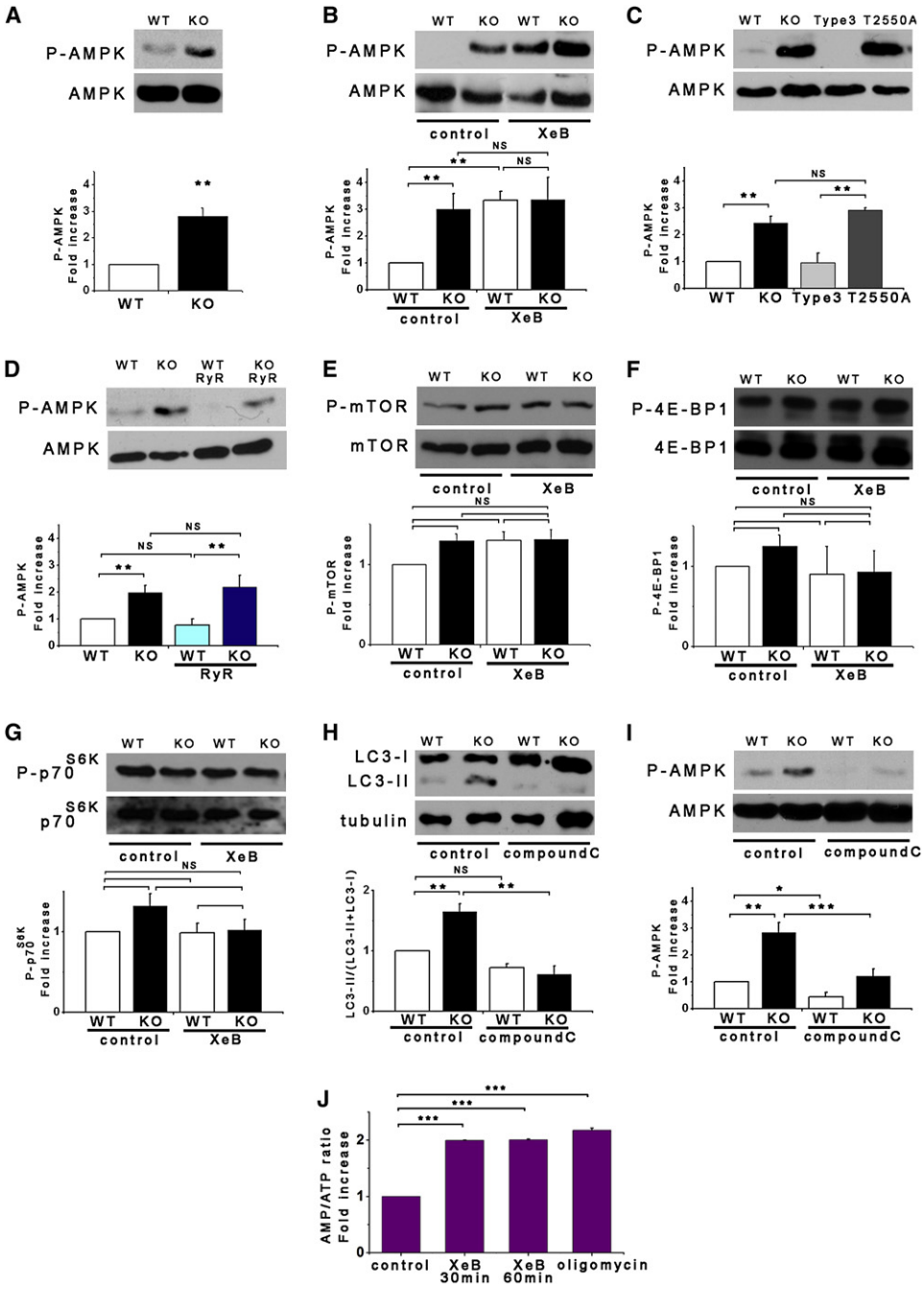

Figure 4. Prosurvival Autophagy Induced by Lack of $InsP_3R$ Ca^{2+} Signaling Is Associated with Activation of AMPK but Not mTOR

(A) DT40-KO have higher levels of P-AMPK than DT40-WT cells. P-AMPK/AMPK expressed as fold increase over WT levels (n = 8).

(B) XeB (2 μM for 1 hr) increases P-AMPK in WT cells to levels observed in KO cells (n = 6).

(C) $InsP_3R$-3 but not Ca^{2+}-impermeable D2550A-$InsP_3R$-3 reduces high P-AMPK in KO cells to control (WT) levels (n = 3).

(D) Expression of RyR-2 fails to reduce P-AMPK in KO cells (n = 3).

(E) mTOR phosphorylation is similar in KO and WT cells and is unaffected by XeB (2 μM for 2 hr). P-mTOR/mTOR levels expressed as fold increase over WT levels (n = 5).

(F and G) Phosphorylation of mTOR substrates 4E-BP1 and $p70^{S6K}$ in KO and WT cells treated or not with 2 μM XeB for 2 hr. P-4E-BP1/4E-BP1 or P-$p70^{S6K}$/$p70^{S6K}$ levels expressed as fold increase over WT levels (n = 5).

(H and I) AMPK inhibition by compound C (CC; 2.5 μM for 1 hr) represses constitutive autophagy and elevated P-AMPK observed in KO cells (n = 5).

(J) XeB (2 μM, 1 hr) increases AMP:ATP ratio in hepatocytes. AMP:ATP ratio expressed as average fold increase (mean ± standard error of the mean [SEM], n = 3) over untreated conditions.

*p < 0.05, **p < 0.01,***p < 0.001; NS: not significant. See also Figure S3.

demonstrate a strict requirement for activation of AMPK to link inhibition of $InsP_3R$-mediated Ca^{2+} signaling to induction of autophagy. Accordingly, a prediction is that cells with AMPK inhibited or knocked down require $InsP_3R$ for survival. In agreement, 14% ± 1% and 28% ± 2% of the HEK-K45R and shRNA cells, respectively, died following 24 hr treatment with XeB, compared with only 3%–5% of cells expressing WT AMPK or empty vector (Figure S3K).

Inhibition of Constitutive $InsP_3R$ Ca^{2+} Release Activity Compromises Cell Bioenergetics

Elevated [AMP] and the requirement for AMPK activation to induce prosurvival autophagy in response to loss of $InsP_3R$ Ca^{2+} signaling suggested that cells lacking this pathway have compromised bioenergetics. We speculated that constitutive low-level $InsP_3R$ Ca^{2+} release promotes oxidative phosphorylation by activation of the ATP synthase (Balaban, 2009; Territo et al., 2000) and/or dehydrogenases to provide reducing equivalents (McCormack et al., 1990). Cells lacking this pathway, as a consequence of $InsP_3R$ deletion or inhibition of its Ca^{2+} release activity, have diminished and uncompensated bioenergetics that are sensed by AMPK that activates autophagy. To test this hypothesis, we attempted to bypass this requirement for $InsP_3R$ Ca^{2+} signaling by enhancing availability of TCA cycle intermediates to increase production of reducing equivalents. Cells were incubated with membrane-permeable methyl-pyruvate (MP) that is oxidized to provide reducing equivalents (NADH) to drive oxidative phosphorylation and ATP production (Lum et al., 2005). Strikingly, MP completely blocked autophagy, and it reduced elevated P-AMPK in DT40-KO cells (Figures 5J and 5K) and in XeB-treated HEK cells (Figures 5L and 5M).

To directly evaluate mitochondrial function, cell O_2 consumption rates (OCR) were measured. Of note, basal OCR was lower by 60% in $InsP_3R$-KO cells compared with WT cells (131 ± 51 versus 44 ± 18 pmole O_2/min/2 × 10^5 cells for WT and KO cells, respectively; Figures 6A and 6B). Maximal OCR was also highly reduced in KO cells (231 ± 48 versus 614 ± 63 pmoleO_2/min/2 × 10^5 for KO and WT cells, respectively; Figures 6A and 6B). Reduced oxidative phosphorylation observed in KO cells was not associated with altered numbers of mitochondria, as evidenced by levels of the mitochondrial marker COX (Figure S2K) and TEM analysis (not shown). These results suggest that oxidative phosphorylation is constitutively compromised in the absence of $InsP_3R$ activity. In contrast, lactate production was enhanced in the KO cells (Figure 6O). To confirm that the observed mitochondrial impairment in KO cells was caused by absence of $InsP_3R$, OCR was measured in XeB-treated WT and KO cells. XeB dramatically reduced both basal and maximal OCR in WT cells, whereas KO cells were unaffected (Figure 6C). Similar observations were made in HEK cells. Basal OCR was reduced by 57% from 304 ± 11 to 130 ± 18 pmole O_2/min/8 × 10^4 cells by XeB, and maximum OCR was reduced 54% from 657 ± 18 to 297 ± 70 pmole O_2/min/8 × 10^4 cells (Figure 6D). Inhibited OCR was rescued by the Ca^{2+} ionophore ionomycin (100 nM; Figure 6E), confirming that availability of Ca^{2+} was specifically limiting for normal oxidative phosphorylation. The number of mitochondria was unchanged by XeB (Figure S4F). Measurements in primary smooth muscle cells and cultured PC12 cells yielded similar results (data not shown). Together these results strongly suggest that basal $InsP_3R$ activity is necessary to provide Ca^{2+} for optimal mitochondrial oxidative phosphorylation. In its absence, mitochondria consume less O_2, reflecting a diminished flux through the electron transport chain.

Mitochondrial Ca^{2+} Uptake Mediates the Effects of $InsP_3R$ Activity on Bioenergetics, AMPK Activity, and Autophagy

Our results indicate that constitutive $InsP_3R$-mediated Ca^{2+}-release in nonstimulated cells is necessary for optimal mitochondrial performance. Accordingly, we hypothesized that induction of autophagy could be recapitulated in cells with functional $InsP_3R$ by preventing mitochondrial Ca^{2+} uptake. Inhibition of mitochondrial Ca^{2+} uptake by the specific Ca^{2+} uniporter blocker Ru360 significantly increased LC3-II in DT40-WT cells, whereas it had no effect in KO cells (Figure 6G). Ru360 also enhanced P-AMPK specifically in WT cells (Figure 6H). These effects of Ru360 are remarkably similar to those of XeB, suggesting that their targets are in the same biochemical pathway. In agreement, effects of XeB and Ru360 on LC3-II and P-AMPK were not additive in DT40 (Figures 6G and 6H) or HEK (Figures 6I and 6J) cells. Furthermore, MP prevented Ru360-induced AMPK activation and autophagy induction (Figures 6K and 6L), as it did with XeB (Figures 5L and 5M). Similar to $InsP_3R$-dependent autophagy, Ru360-induced autophagy was mTOR independent (Figures S4I and S4J). Autophagy induced by Ru360 was associated with impaired mitochondrial bioenergetics. As with XeB, Ru360 decreased basal OCR by over 50% in both DT40-WT cells and HEK cells (Figures 6M and 6N). In contrast, the constitutively lower basal OCR in DT40-KO cells was unaffected (Figure 6M). Likewise, maximal OCR also was reduced by 50%–60% in both DT40-WT and HEK cells (Figures 6M and 6N). Inhibition of OCR by Ru360 was reversed by ionomycin (100 nM; Figure 6F), again confirming that availability of Ca^{2+} was specifically limiting for normal oxidative phosphorylation.

Pyruvate Dehydrogenase Activity Couples Constitutive $InsP_3R$-Mediated Ca^{2+} Release to Oxidative Phosphorylation

Mitochondrial matrix Ca^{2+} can regulate oxidative phosphorylation at several sites, including the F_1F_0-ATPase and several dehydrogenases, including pyruvate dehydrogenase (PDH) (Balaban, 2009; Territo et al., 2000), a major switch that links glycolysis to the tricarboxylic acid cycle by irreversible decarboxylation of pyruvate. Phosphorylation of PDH by pyruvate dehydrogenase kinase suppresses its activity whereas dephosphorylation by Ca^{2+}-dependent pyruvate phosphatase enhances it (Patel and Korotchkina, 2006). PDH was hyperphosphorylated in DT40-KO cells (Figure 7A) and in XeB-treated HEK cells (Figure 7B). Importantly, inhibition of PDH kinases in KO cells by dichloroacetic acid (DCA, 2 mM) (Michelakis et al., 2008) reduced PDH phosphorylation (Figure 7C), restored OCR (Figure 7D), and reduced autophagy (Figure 7E) to control levels. These results suggest that mitochondrial respiration is compromised in the absence of $InsP_3R$ function and implicate insufficient PDH activity as an important component.

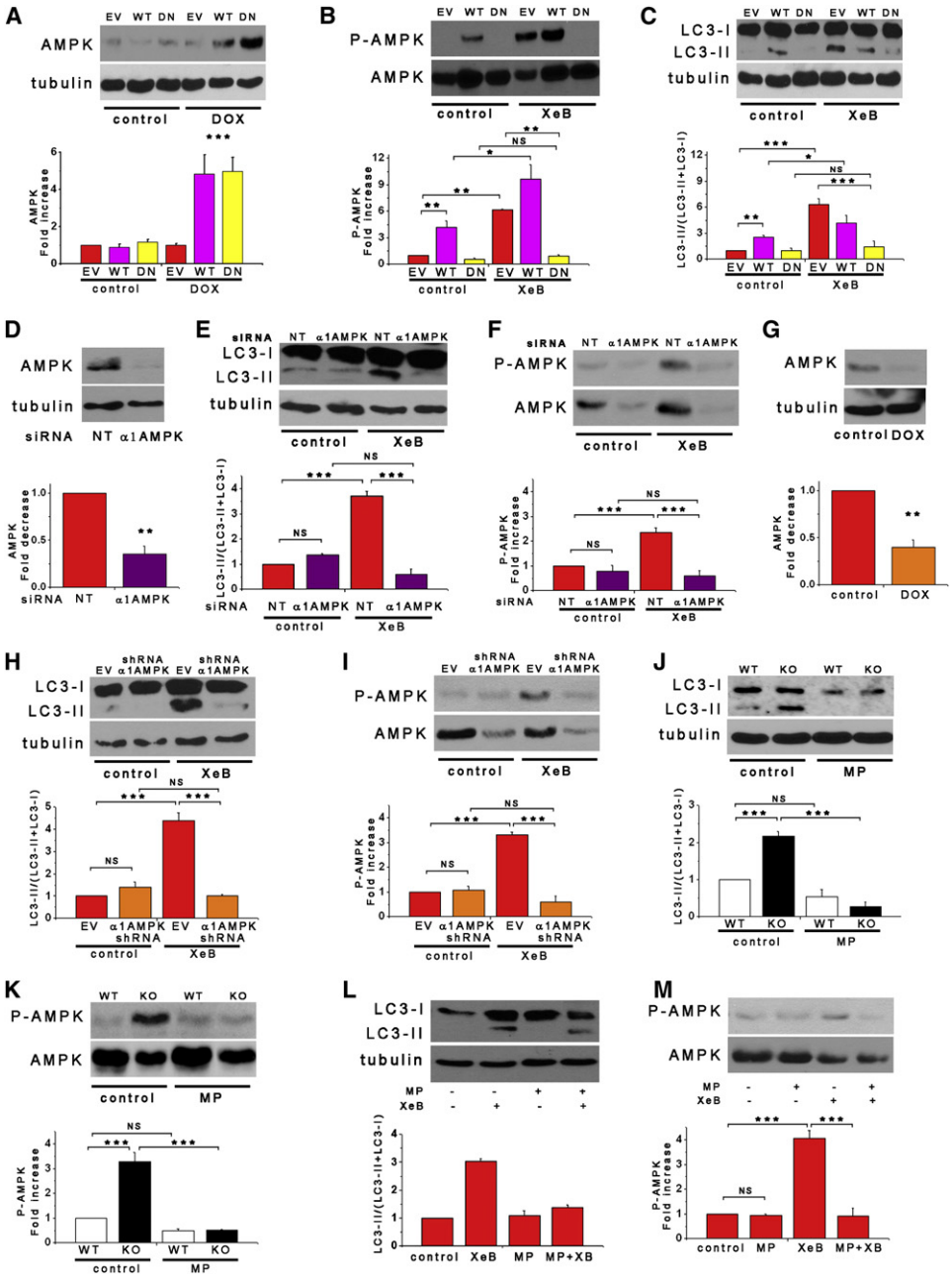

Figure 5. Prosurvival Autophagy Induced by Lack of InsP$_3$R Ca^{2+} Signaling Is Mediated by AMPK

(A) α1-AMPK expression in HEK293 cells stably expressing DOX-inducible WT or dominant-negative (DN) α1-AMPK in presence or absence of DOX. Cells transfected with empty vector (EV) used as control. AMPK/tubulin expressed as fold increase over basal levels (DOX untreated) (n = 6).

(B and C) XeB (2 μM for 1 hr) failed to trigger either autophagy or AMPK phosphorylation in cells expressing DN-AMPK. Overexpression of WT α1-AMPK increased autophagy (n = 6).

(D) α1-AMPK levels in HEK cells transiently transfected with α1-AMPK or irrelevant (NT) siRNA (n = 3).

(E and F) XeB fails to induce autophagy or P-AMPK in cells transiently transfected with α1-AMPK siRNA (n = 3).

(G) HEK293 cells stably expressing inducible α1-AMPK shRNA were exposed to DOX for 72 hr (n = 3).

(H and I) XeB fails to induce autophagy and P-AMPK in cells expressing inducible α1-AMPK shRNA (n = 3).

(J–M) Treatment of DT40-KO (J and K) and HEK293 (L and M) cells with methyl-pyruvate (MP; 5 μM for 1 hr) reduced autophagy and AMPK hyperphosphorylation (n = 3).

*p < 0.05, **p < 0.01, ***p < 0.001; NS, not significant. See also Figure S3 and Figure S4.

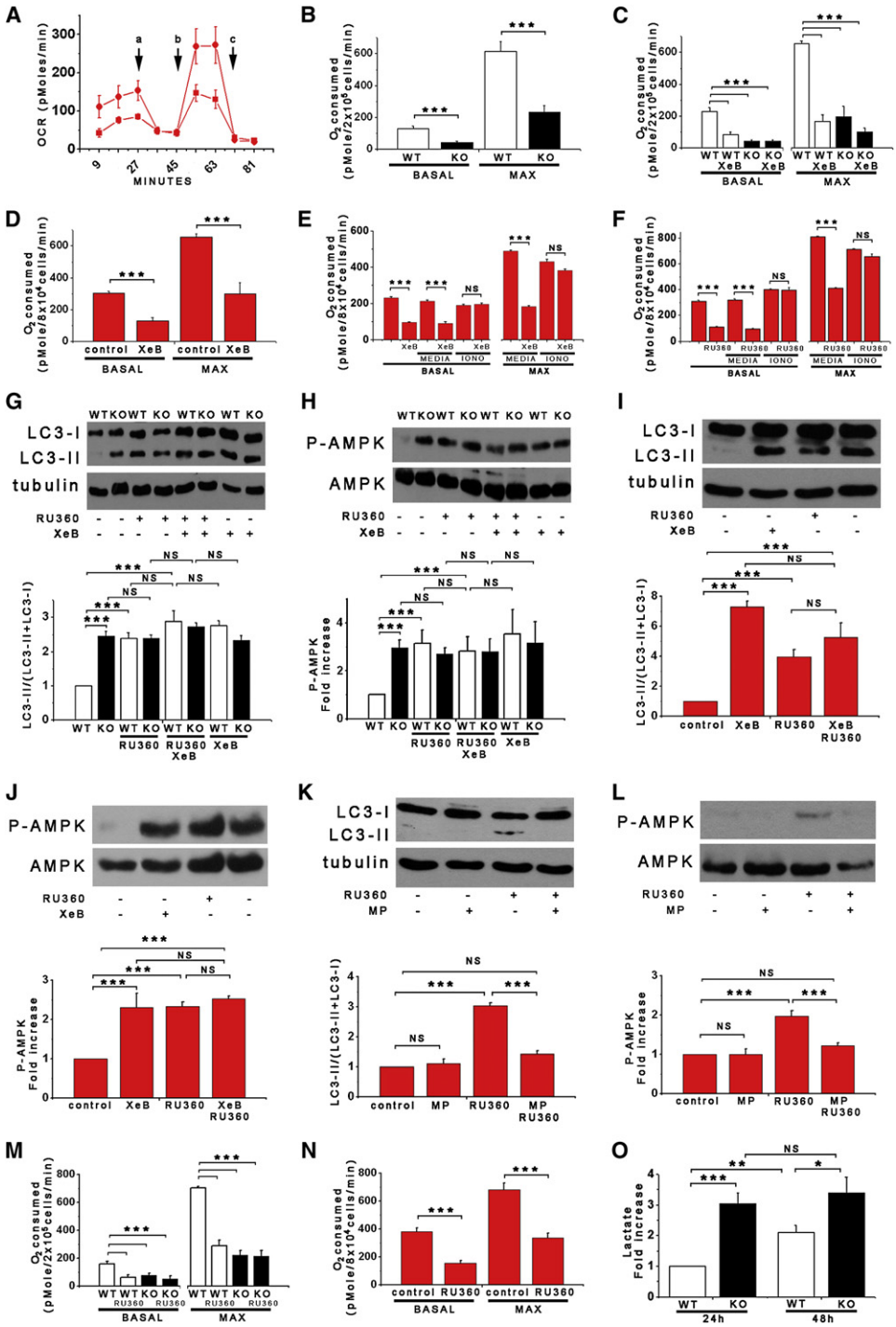

Figure 6. Lack of InsP$_3$R Ca^{2+} Signaling and Inhibition of Mitochondrial Ca^{2+} Uptake Are in the Same Pathway that Regulates Bioenergetics and Autophagy

(A) Oxygen consumption rates (OCR) in WT (red) and KO (black) DT40 cells exposed sequentially to (a) oligomycin, (b) FCCP, and (c) rotenone plus myzothiazol.

(B) Basal and maximal OCR in DT40-WT and DT40-KO cells (n = 3).

(C and D) Basal and maximal OCR in DT40 and HEK293 cells treated or not with XeB (2 μM for 1 hr) (n = 3).

(E and F) The Ca^{2+} ionophore ionomycin (100 nM) reversed inhibitory effects of XeB (E) and Ru360 (F) on OCR.

(G–J) Effects of inhibition of mitochondrial Ca^{2+} uptake by Ru360 (10 μM for 1 hr) in absence or presence of XeB on autophagy and P-AMPK in DT40 (G and H) and HEK293 (I and J) cells (n = 3).

(K and L) Effects of methyl-pyruvate (MP, 5 μM) on autophagy and P-AMPK evoked by 10 μM Ru360 in HEK293 cells (n = 3).

Constitutive $InsP_3R$-Mediated Low-Level Ca^{2+} Signaling Is Present in Cells in Normal Growth Medium

Our results suggest that constitutive $InsP_3R$ Ca^{2+} release is necessary for ongoing support of optimal mitochondrial function. We speculated that the important Ca^{2+} signals are highly localized, are stochastic, and occur throughout unstimulated cells to ensure ongoing mitochondrial Ca^{2+} uptake to support whole-cell respiration. To observe such signals, we turned to human neuroblastoma SH-SY5Y cells because Ca^{2+} release associated with single $InsP_3R$ channel openings can be visualized in them (Smith et al., 2009). We first confirmed that autophagy was similarly regulated by $InsP_3R$ in these cells as in the many cell types studied above. RNAi knockdown of $InsP_3R$-1, the dominant isoform in these cells (Wojcikiewicz and Luo, 1998), by ~80% (Figure 7F) or treatment with XeB significantly increased LC3-II (Figures 7G and 7I) and P-AMPK (Figures 7H and 7J). Basal and maximal OCR were inhibited by 33% by XeB (Figure 7K). Ru360 induced autophagy and elevated P-AMPK (Figures S5A and S5B). Thus, as in the other cell types examined in this study, SH-SY5Y cells rely on constitutive Ca^{2+} transfer from the endoplasmic reticulum (ER) to mitochondria, mediated by $InsP_3R$ and the uniporter, to maintain normal cell bioenergetics.

To image the hypothesized constitutive Ca^{2+} signals, we employed total internal reflection fluorescence (TIRF) microscopy with high temporal and spatial resolution (Demuro and Parker, 2006). With perfusion in normal medium, 96% of cells showed spontaneous miniature Ca^{2+} release events (Figure 7L, bottom trace, Figure S5D, and Movie S1), likely representing openings of a single or few $InsP_3R$ channels (Smith and Parker, 2009; Smith et al., 2009), at a frequency of 22.5 ± 5 events/cell/min (Figure 7M and Figure S5D), although many cells displayed >40 events/cell/min (not shown). Transfer to Hank's medium suppressed these events (Figure 7L, upper trace), with only 58% of cells displaying Ca^{2+} release activity with a 10-fold reduced frequency (2.9 ± 0.7 events/cell/min) (Figure 7M), with the most active cells displaying at most 10 events/cell/min (not shown). Amplitudes of release events were not different in the two conditions (Figure S5C). Treatment of cells in normal medium with XeB had a similar effect: after XeB only 56% of cells displayed spontaneous Ca^{2+} release activity with only 4.6 ± 1.5 events/cell/min compared with 21.5 ± 2 events/cell/min observed in untreated cells. The inhibitory effects of XeB were reversible (Figure 7N).

DISCUSSION

The most significant finding of our studies is that constitutive low-level $InsP_3R$-mediated Ca^{2+} release is essential for maintenance of optimal cellular bioenergetics under normal basal conditions. In all of several cell types examined, cells become metabolically compromised in the absence of this ongoing Ca^{2+} release activity as a result of diminished Ca^{2+} uptake by mitochondria. Previous studies have suggested that agonist-induced $InsP_3R$ Ca^{2+} signals can be transmitted to mitochondria where they can enhance mitochondrial function (Rizzuto et al., 1998; Spat et al., 2008). Our studies demonstrate that mitochondrial uptake of $InsP_3R$-released Ca^{2+} is required for basal mitochondrial bioenergetics in the absence of specific agonist stimulation, and it is fundamentally essential for maintenance of normal cellular bioenergetics. This ongoing Ca^{2+} transfer from ER to mitochondria maintains optimal mitochondrial bioenergetics by supporting oxidative phosphorylation, at least in part by providing sufficient reducing equivalents. Reduction of this Ca^{2+} transfer results in reduced ATP production and activation of AMPK, which promotes autophagy as a prosurvival mechanism even in the presence of sufficient amino acids to maintain cellular mTOR activation (Figure S6). These results reveal a heretofore unexpected essential role for constitutive low-level $InsP_3R$-mediated Ca^{2+} delivery to mitochondria to preserve normal cellular bioenergetics.

Constitutive $InsP_3R$ Ca^{2+} Release Is Required to Inhibit Prosurvival Autophagy in Normal Conditions

The $InsP_3R$ has been implicated in mTOR-independent autophagy (Criollo et al., 2007; Sarkar et al., 2005; Vicencio et al., 2009; Williams et al., 2008). Our results identify a molecular mechanism for this regulation that involves AMPK and impaired cellular bioenergetics when $InsP_3R$ activity is compromised. Inhibition of autophagy by expression of WT but not mutants deficient in Ca^{2+} release that nevertheless have similar binding to Beclin-1 demonstrates that $InsP_3R$ suppresses autophagy by its ability to release Ca^{2+} into the cytoplasm. The role of released Ca^{2+} was unrelated to a Ca^{2+} requirement for nutrient uptake, as this was not diminished, but was rather somewhat enhanced in cells lacking the $InsP_3R$. Enhanced nutrient uptake, activation of AMPK, and induction of prosurvival autophagy associated with inhibition of $InsP_3R$ Ca^{2+} release are responses normally observed in cells in nutrient-deficient conditions. Thus, lack of constitutive $InsP_3R$ Ca^{2+} signaling activates a bone fide prosurvival response to bioenergetic stress despite presence of nutrients and growth factors. That autophagy was activated as a prosurvival mechanism was confirmed by responses of autophagy-deficient HEK cells to $InsP_3R$ inhibition and of DT40 cells to 3MA, which caused significant death of $InsP_3R$ activity-deficient cells compared with their WT counterparts, and by the toxicity of XeB in autophagy-deficient Atg5 null cells. In addition, $InsP_3R$-deficient cells were much more resistant to actual nutrient deprivation than WT cells and recovered much more quickly when nutrients were resupplied, all consistent with activation of autophagy in the absence of $InsP_3R$ Ca^{2+} release as a prosurvival strategy.

Inhibition of Constitutive $InsP_3R$ Ca^{2+} Release Compromises Cell Bioenergetics

Several observations indicate that $InsP_3R$ Ca^{2+} release in normal medium is necessary to support optimal cellular bioenergetics.

(M and N) Effects of mitochondrial Ca^{2+} uptake inhibition by Ru360 on basal and maximum OCR in DT40 (M) and HEK293 (N) cells (n = 3).
(O) Lactate generation in WT and KO cells after 24 hr in normal media (n = 3).
***$p < 0.001$; NS, not significant. See also Figure S4.

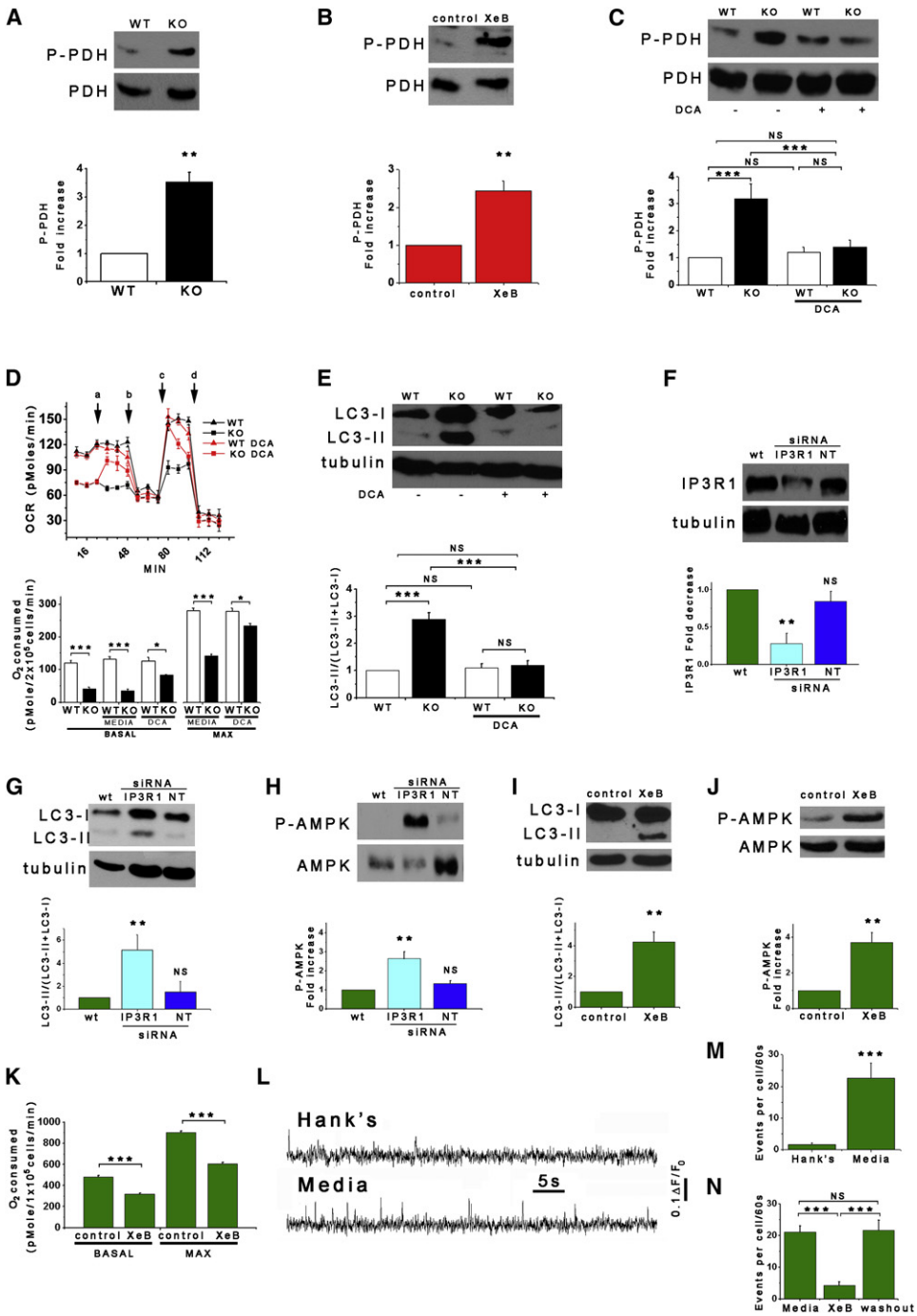

Figure 7. Normal Growth Medium Supports Constitutive $InsP_3R$ Ca^{2+} Release

(A and B) DT40-KO cells and XeB-treated HEK293 cells have higher levels of phospho-PDH (n = 3).

(C–E) DCA treatment normalizes PDH hyperphosphorylation (C; 2 mM for 1 hr), enhances OCR (D; added acutely at "a"), and suppresses autophagy (E; 2 mM for 1 hr) in KO cells to WT levels (n = 3).

(F) Effect of transient transfection (48 hr) with specific or irrelevant (NT) siRNA on $InsP_3R$-1 expression in SH-SY5Y cells. $InsP_3R$-1/tubulin (n = 3) was expressed relative to basal levels.

(G–J) Effects of $InsP_3R$-1 knockdown (G and H) or XeB (10 μM, 1 hr) (I and J) on autophagy and P-AMPK in SH-SY5Y cells (n = 3).

(K) Effects of $InsP_3R$-1 knockdown on basal and maximum OCR in SH-SY5Y cells (n = 3).

(L) Representative fluorescence recordings of Ca^{2+} release events in unstimulated SH-SY5Y cells in either Hank's solution or normal culture media.

(M) Quantification of Ca^{2+} release events in SH-SY5Y cells exposed either to Hank's or normal media (n = 3 experiments).

(N) Effects of XeB (10 μM for 30 min) on spontaneous Ca^{2+} release events recorded in SH-SY5Y cells in normal media (n = 3 experiments).

**p < 0.01, ***p < 0.001. See also Figure S5 and Movie S1.

First, inhibition of $InsP_3R$ activity or expression resulted in AMPK activation. AMPK is a highly sensitive indicator of cellular energy status, whose activity increases under conditions of metabolic stress that elevate the cytoplasmic AMP:ATP ratio (Hardie, 2007). In agreement, inhibition of $InsP_3R$ increased [AMP] and AMP:ATP. AMPK activation was blocked by MP, consistent with reduced mitochondrial ATP production in cells with diminished $InsP_3R$ Ca^{2+} release activity. This conclusion is also supported by OCR measurements that directly interrogate the rate of electron transfer to oxygen in complex IV of the electron transport chain. Basal OCR was significantly reduced in cells with $InsP_3R$ activity diminished, indicating that ATP production was reduced. This was true under short-term conditions, when channel activity was inhibited with XeB, and under chronic conditions, exemplified in DT40-KO cells where no compensatory upregulation of OCR was evident. Rather, enhanced lactate production suggests that increased glycolysis, in addition to autophagy, were compensatory responses to compromised cell bioenergetics.

Mitochondrial Ca^{2+} Uptake Mediates Effects of $InsP_3R$ Activity on Bioenergetics

Maximal OCR in uncoupled mitochondria was also reduced in cells lacking $InsP_3R$ activity. Failure of an uncoupler to normalize OCR between cells having or lacking $InsP_3R$ activity suggests that the mitochondrial deficiency resides in their inability to produce sufficient NADH to maintain electron flow through the respiratory complex. Whether this deficiency also accounts for reduced basal respiration is not as clear. However, PDH became hyperphosphorylated (inactivated) in cells lacking $InsP_3R$ activity, and reversal of this by inhibition of PDH kinases restored normal oxidative phosphorylation and inhibited constitutive autophagy. These results are most consistent with $InsP_3R$ activity being linked to regulation of cell bioenergetics through constitutive Ca^{2+}-dependent regulation of the PDH phosphatase. PDH, and two other rate-limiting metabolic enzymes, α-ketoglutarate- and isocitrate-dehydrogenases, are activated by matrix Ca^{2+}, generating NADH required for ATP synthesis (McCormack et al., 1990). Ca^{2+} permeation into mitochondria is rate limited at the inner membrane, where uptake occurs through the uniporter channel, driven by the membrane voltage generated by electron transport in normally respiring mitochondria (Spat et al., 2008). Ca^{2+} uptake by mitochondria in vitro occurs over a range of 1–100 μM Ca^{2+} (Spat et al., 2008; Szabadkai and Duchen, 2008). Nevertheless, $InsP_3$-linked agonists that generate sub-μM global $[Ca^{2+}]_i$ elevations trigger large increases in mitochondrial matrix $[Ca^{2+}]$ (Spat et al., 2008) because of close appositions between mitochondria and ER supported by physical linkages (Csordas et al., 2006; Rizzuto et al., 1998). In these confined spaces, Ca^{2+} released through $InsP_3R$ can reach levels sufficient for permeation through the uniporter (Rizzuto et al., 1998). In our studies, the uniporter inhibitor Ru360 elicited all of the cellular responses observed in cells with diminished $InsP_3R$ Ca^{2+} release. Thus, Ru360 inhibited OCR, activated AMPK, and induced autophagy. Ru360 was without effect on cells with $InsP_3R$ Ca^{2+} release compromised, indicating that ER Ca^{2+} release and mitochondrial Ca^{2+} uptake are in the same pathway that impinges on cell bioenergetics and autophagy. Importantly, the metabolic deficits induced by Ru360, like those induced by disrupted $InsP_3R$ function, were completely reversed by ionomycin and MP, reinforcing the conclusion that a major defect in cells lacking $InsP_3R$ activity is insufficient Ca^{2+}-dependent NADH production to support electron transport.

Whereas the PLC/$InsP_3$/Ca^{2+} system has been widely considered within the context of agonist stimulation, most studies have used basic salt solutions lacking nutrients and growth factors. The experimental rationale for use of such solutions is obvious, but they are unphysiological and, indeed, similar to those used to induce starvation-mediated autophagy. Cells in their normal milieu are bathed in a variety of factors, some of which impinge on the PLC/$InsP_3$ system. It is likely that low $[InsP_3]_I$ exist in all cells in vivo and can be expected to drive low-level $InsP_3R$ Ca^{2+} release activity. We confirmed this by demonstrating that whereas spontaneous $InsP_3R$-mediated Ca^{2+} release events are rare in saline buffer, they are quite frequent in cells bathed in medium containing nutrient and growth factors that more closely mimic in vivo conditions. These events were transient and highly localized, consistent with stochastic release from one to a few $InsP_3Rs$ throughout the cytoplasm (Smith and Parker, 2009; Smith et al., 2009). Optimal production of NADH in mitochondria is achieved by repetitive transient Ca^{2+} spikes (Hajnoczky et al., 1995; Jouaville et al., 1999; Robb-Gaspers et al., 1998; Szabadkai and Duchen, 2008), whereas sustained Ca^{2+} release can be associated with mitochondrial Ca^{2+}overload that could activate the mitochondrial transition pore, with possible detrimental consequences including apoptosis and necrosis (Szalai et al., 1999).

In summary, we have identified an essential cellular process that is required for efficient mitochondrial respiration and maintenance of normal cell bioenergetics and that involves constitutive Ca^{2+} transfer from the ER to mitochondria mediated by the $InsP_3R$. Because of the fundamental importance of cellular bioenergetics control in normal cellular physiology and pathophysiology, as well as the role of autophagy in diverse human pathologies (Levine and Kroemer, 2008), identification of this process has broad implications.

EXPERIMENTAL PROCEDURES

Reagents, Cell Culture, and Transfection

Details can be found in Extended Experimental Procedures.

Detection of Autophagy

Western Blot

Details can be found in Extended Experimental Procedures.

Electron Microscopy

Cells were fixed in 2.5% glutaraldehyde in 0.1M cacodylate buffer, post-fixed in 2% osmium tetroxide, dehydrated and embedded in Epon, and examined with a high-voltage electron microscope (Philips EM 410). Autophagosomes were identified by classic morphologic features of size >0.5 μm, presence of a double-limiting membrane, and heterogeneous intralumenal contents (Eskelinen, 2008).

Confocal Microscopy

GFP-LC3-expressing cells were fixed with 4% paraformaldehyde and GFP fluorescence was visualized with a Zeiss Axiovert 510 LSM Pascal confocal microscope using a 488 nm laser line.

Nutrient Uptake

DT40 cells were seeded (5×10^4 cells ml^{-1}) in complete media and cultured in standard conditions (37°C, 95%/5% air/CO_2). Media in flasks lacking cells were used to control for nutrient degradation. Media were analyzed by a metabolite analyzer (Novaflex BioProfiles). Cells were counted daily, and nutrient disappearance from the media was normalized to cell number.

Glucose Transport

DT40 cells were washed with Krebs-BSA buffer, preincubated or not with cytochalasin B (10 min), and incubated for 10 min at 37°C with ^{3}H-2-deoxyglucose (DOG = 10 mM). The reaction was stopped by placing it on ice. Samples were spun, decanted, lysed in 1% triton x-100, and cell ^{3}H quantified.

Single-Channel $InsP_3R$ Recording

$InsP_3R$ single-channel recording by patch-clamp electrophysiology of isolated DT40 cell nuclei was performed as described (White et al., 2005). Ion selectivity was performed as described (Mak and Foskett, 1994), with reversal potentials corrected for liquid junction potentials.

Cell Viability

Viability assays were performed as described (Shimizu et al., 2004). Details can be found in Extended Experimental Procedures.

Oxygen Consumption

Oxygen consumption rate (OCR) was measured in at 37°C using an XF24 extracellular analyzer (Seahorse Bioscience). Details can be found in Extended Experimental Procedures.

Calcium Imaging

Details can be found in Extended Experimental Procedures.

Quantification of Adenine Nucleotides

Nucleotides were extracted from primary hepatocytes using perchloric acid, neutralized, and frozen for subsequent HPLC analysis (Kochanowski et al., 2006). AMP, ADP, and ATP in extracted samples were quantified using ion-pair reverse-phase HPLC, with a C18 RP column, under isocratic elution conditions in 200 mM phosphate, 5 mM tetrabutylammonium phosphate, and 3% acetonitrile.

Analysis and Statistics

All data summarized as mean ± SEM; significance of differences was assessed using unpaired t tests. Differences were accepted as significant at the 95% level ($p < 0.05$).

SUPPLEMENTAL INFORMATION

Supplemental Information includes Extended Experimental Procedures, six figures, and one movie and can be found with this article online at doi:10.1016/j.cell.2010.06.007.

ACKNOWLEDGMENTS

We thank Dr. Robert Balaban for helpful discussions. This work was supported by NIH grants GM/DK56328 and MH059937 (J.K.F.), DK075048 (K.R.H.), CA099179 and CA092660 (C.T.), GM48071 (I.P.), and GM065830 (J.K.F. and I.P.). We thank the University of Pennsylvania Institute for Diabetes, Obesity and Metabolism (P30-DK19535) for assistance. C.C. was supported by an award from the American Heart Association. R.A.M. was supported by DK079572.

Received: October 14, 2009
Revised: March 26, 2010
Accepted: May 20, 2010
Published: July 22, 2010

REFERENCES

Balaban, R.S. (1990). Regulation of oxidative phosphorylation in the mammalian cell. Am. J. Physiol. *258*, C377–C389.

Balaban, R.S. (2009). The role of Ca^{2+} signaling in the coordination of mitochondrial ATP production with cardiac work. Biochim. Biophys. Acta *1787*, 1334–1341.

Balaban, R.S., Nemoto, S., and Finkel, T. (2005). Mitochondria, oxidants, and aging. Cell *120*, 483–495.

Bhalla, V., Oyster, N.M., Fitch, A.C., Weingarten, M.A., Neumann, D., Schlattner, U., Pearce, D., and Hallows, K.R. (2006). AMP-activated kinase inhibits the epithelial Na^+ channel through functional regulation of the ubiquitin ligase Nedd4-2. J. Biol. Chem. *281*, 26159–26169.

Brown, G.C. (1992). Control of respiration and ATP synthesis in mammalian mitochondria and cells. Biochem. J. *284*, 1–13.

Criollo, A., Maiuri, M.C., Tasdemir, E., Vitale, I., Fiebig, A.A., Andrews, D., Molgó, J., Diaz, J., Lavandero, S., Harper, F., et al. (2007). Regulation of autophagy by the inositol trisphosphate receptor. Cell Death Differ. *14*, 1029–1039.

Csordas, G., Renken, C., Varnai, P., Walter, L., Weaver, D., Buttle, K.F., Balla, T., Mannella, C.A., and Hajnoczky, G. (2006). Structural and functional features and significance of the physical linkage between ER and mitochondria. J. Cell Biol. *174*, 915–921.

Demuro, A., and Parker, I. (2006). Imaging single-channel calcium microdomains. Cell Calcium *40*, 413–422.

Eskelinen, E.L. (2008). To be or not to be? Examples of incorrect identification of autophagic compartments in conventional transmission electron microscopy of mammalian cells. Autophagy *4*, 257–260.

Fill, M., and Copello, J.A. (2002). Ryanodine receptor calcium release channels. Physiol. Rev. *82*, 893–922.

Gustafsson, A.B., and Gottlieb, R.A. (2008). Heart mitochondria: gates of life and death. Cardiovasc. Res. *77*, 334–343.

Hajnoczky, G., Robb-Gaspers, L.D., Seitz, M.B., and Thomas, A.P. (1995). Decoding of cytosolic calcium oscillations in the mitochondria. Cell *82*, 415–424.

Hallows, K.R., Alzamora, R., Li, H., Gong, F., Smolak, C., Neumann, D., and Pastor-Soler, N.M. (2009). AMP-activated protein kinase inhibits alkaline pH- and PKA-induced apical vacuolar H^+-ATPase accumulation in epididymal clear cells. Am. J. Physiol. *296*, C672–C681.

Hardie, D.G. (2007). AMP-activated/SNF1 protein kinases: conserved guardians of cellular energy. Nat. Rev. Mol. Cell Biol. *8*, 774–785.

Huttemann, M., Lee, I., Kreipke, C.W., and Petrov, T. (2008). Suppression of the inducible form of nitric oxide synthase prior to traumatic brain injury improves cytochrome c oxidase activity and normalizes cellular energy levels. Neuroscience *151*, 148–154.

Jaimovich, E., Mattei, C., Liberona, J.L., Cárdenas, C., Estrada, M., Barbier, J., Debitus, C., Laurent, D., and Molgó, J. (2005). Xestospongin B, a competitive inhibitor of IP_3-mediated Ca^{2+} signalling in cultured rat myotubes, isolated myonuclei, and neuroblastoma (NG108-15) cells. FEBS Lett. *579*, 2051–2057.

Jouaville, L.S., Pinton, P., Bastianutto, C., Rutter, G.A., and Rizzuto, R. (1999). Regulation of mitochondrial ATP synthesis by calcium: evidence for a long-term metabolic priming. Proc. Natl. Acad. Sci. USA *96*, 13807–13812.

Kimball, S.R. (2006). Interaction between the AMP-activated protein kinase and mTOR signaling pathways. Med. Sci. Sports Exerc. *38*, 1958–1964.

Klionsky, D.J. (2007). Autophagy: from phenomenology to molecular understanding in less than a decade. Nat. Rev. Mol. Cell Biol. *8*, 931–937.

Klionsky, D.J., Abeliovich, H., Agostinis, P., Agrawal, D.K., Aliev, G., Askew, D.S., Baba, M., Baehrecke, E.H., Bahr, B.A., Ballabio, A., et al. (2008). Guidelines for the use and interpretation of assays for monitoring autophagy in higher eukaryotes. Autophagy *4*, 151–175.

Kochanowski, N., Blanchard, F., Cacan, R., Chirat, F., Guedon, E., Marc, A., and Goergen, J.L. (2006). Intracellular nucleotide and nucleotide sugar

contents of cultured CHO cells determined by a fast, sensitive, and high-resolution ion-pair RP-HPLC. Anal. Biochem. *348*, 243–251.

Levine, B., and Kroemer, G. (2008). Autophagy in the pathogenesis of disease. Cell *132*, 27–42.

Lum, J.J., Bauer, D.E., Kong, M., Harris, M.H., Li, C., Lindsten, T., and Thompson, C.B. (2005). Growth factor regulation of autophagy and cell survival in the absence of apoptosis. Cell *120*, 237–248.

Mak, D.O., and Foskett, J.K. (1994). Single-channel inositol 1,4,5-trisphosphate receptor currents revealed by patch clamp of isolated Xenopus oocyte nuclei. J. Biol. Chem. *269*, 29375–29378.

Mattson, M.P., Gleichmann, M., and Cheng, A. (2008). Mitochondria in neuroplasticity and neurological disorders. Neuron *60*, 748–766.

McCormack, J.G., Halestrap, A.P., and Denton, R.M. (1990). Role of calcium ions in regulation of mammalian intramitochondrial metabolism. Physiol. Rev. *70*, 391–425.

Meijer, A.J. (2008). Amino acid regulation of autophagosome formation. Methods Mol. Biol. *445*, 89–109.

Michelakis, E.D., Webster, L., and Mackey, J.R. (2008). Dichloroacetate (DCA) as a potential metabolic-targeting therapy for cancer. Br. J. Cancer *99*, 989–994.

Nicklin, P., Bergman, P., Zhang, B., Triantafellow, E., Wang, H., Nyfeler, B., Yang, H., Hild, M., Kung, C., Wilson, C., et al. (2009). Bidirectional transport of amino acids regulates mTOR and autophagy. Cell *136*, 521–534.

Patel, M.S., and Korotchkina, L.G. (2006). Regulation of the pyruvate dehydrogenase complex. Biochem. Soc. Trans. *34*, 217–222.

Rizzuto, R., Pinton, P., Carrington, W., Fay, F.S., Fogarty, K.E., Lifshitz, L.M., Tuft, R.A., and Pozzan, T. (1998). Close contacts with the endoplasmic reticulum as determinants of mitochondrial Ca^{2+} responses. Science *280*, 1763–1766.

Robb-Gaspers, L.D., Burnett, P., Rutter, G.A., Denton, R.M., Rizzuto, R., and Thomas, A.P. (1998). Integrating cytosolic calcium signals into mitochondrial metabolic responses. EMBO J. *17*, 4987–5000.

Sarkar, S., Floto, R.A., Berger, Z., Imarisio, S., Cordenier, A., Pasco, M., Cook, L.J., and Rubinsztein, D.C. (2005). Lithium induces autophagy by inhibiting inositol monophosphatase. J. Cell Biol. *170*, 1101–1111.

Shimizu, S., Kanaseki, T., Mizushima, N., Mizuta, T., Arakawa-Kobayashi, S., Thompson, C.B., and Tsujimoto, Y. (2004). Role of Bcl-2 family proteins in a non-apoptotic programmed cell death dependent on autophagy genes. Nat. Cell Biol. *6*, 1221–1228.

Smeitink, J.A., Zeviani, M., Turnbull, D.M., and Jacobs, H.T. (2006). Mitochondrial medicine: a metabolic perspective on the pathology of oxidative phosphorylation disorders. Cell Metab. *3*, 9–13.

Smith, I.F., and Parker, I. (2009). Imaging the quantal substructure of single IP_3R channel activity during Ca^{2+} puffs in intact mammalian cells. Proc. Natl. Acad. Sci. USA *106*, 6404–6409.

Smith, I.F., Wiltgen, S.M., and Parker, I. (2009). Localization of puff sites adjacent to the plasma membrane: functional and spatial characterization of Ca^{2+} signaling in SH-SY5Y cells utilizing membrane-permeant caged IP_3. Cell Calcium *45*, 65–76.

Spat, A., Szanda, G., Csordas, G., and Hajnoczky, G. (2008). High- and low-calcium-dependent mechanisms of mitochondrial calcium signalling. Cell Calcium *44*, 51–63.

Sugawara, H., Kurosaki, M., Takata, M., and Kurosaki, T. (1997). Genetic evidence for involvement of type 1, type 2 and type 3 inositol 1,4,5-trisphosphate receptors in signal transduction through the B-cell antigen receptor. EMBO J. *16*, 3078–3088.

Szabadkai, G., and Duchen, M.R. (2008). Mitochondria: the hub of cellular Ca^{2+} signaling. Physiology *23*, 84–94.

Szalai, G., Krishnamurthy, R., and Hajnoczky, G. (1999). Apoptosis driven by IP(3)-linked mitochondrial calcium signals. EMBO J. *18*, 6349–6361.

Territo, P.R., Mootha, V.K., French, S.A., and Balaban, R.S. (2000). Ca^{2+} activation of heart mitochondrial oxidative phosphorylation: role of the F(0)/F(1)-ATPase. Am. J. Physiol. *278*, C423–C435.

Vander Heiden, M.G., Cantley, L.C., and Thompson, C.B. (2009). Understanding the Warburg effect: the metabolic requirements of cell proliferation. Science *324*, 1029–1033.

Vicencio, J.M., Ortiz, C., Criollo, A., Jones, A.W., Kepp, O., Galluzzi, L., Joza, N., Vitale, I., Morselli, E., Tailler, M., et al. (2009). The inositol 1,4,5-trisphosphate receptor regulates autophagy through its interaction with Beclin 1. Cell Death Differ. *16*, 1006–1017.

Wallace, D.C. (2005). Mitochondria and cancer: Warburg addressed. Cold Spring Harb. Symp. Quant. Biol. *70*, 363–374.

White, C., Li, C., Yang, J., Petrenko, N.B., Madesh, M., Thompson, C.B., and Foskett, J.K. (2005). The endoplasmic reticulum gateway to apoptosis by Bcl-X_L modulation of the $InsP_3R$. Nat. Cell Biol. *7*, 1021–1028.

Williams, A., Sarkar, S., Cuddon, P., Ttofi, E.K., Saiki, S., Siddiqi, F.H., Jahreiss, L., Fleming, A., Pask, D., Goldsmith, P., et al. (2008). Novel targets for Huntington's disease in an mTOR-independent autophagy pathway. Nat. Chem. Biol. *4*, 295–305.

Wojcikiewicz, R.J., and Luo, S.G. (1998). Differences among type I, II, and III inositol-1,4,5-trisphosphate receptors in ligand-binding affinity influence the sensitivity of calcium stores to inositol-1,4,5-trisphosphate. Mol. Pharmacol. *53*, 656–662.

Cell

EXTENDED EXPERIMENTAL PROCEDURES

Reagents

Antibodies

From Cell Signaling Technology: Phospho-α1-AMPK (Thr172), Phospho-mTOR (Ser2448), mTOR, Phospho-p70^{S6K} (Thr389), Phospho-4E-BP1 (Thr37/46), and 4E-BP1. From Millipore: α1-AMPK. From ZYMED Laboratories: β-tubulin. From Santa Cruz Biotechnology: p70^{S6K}, Beclin 1. From MitoSciences: cytochrome c oxidase (COX). From Novus Biologicals: Phospho-pyruvate dehydrogenase E1 alpha (Ser293). From Invitrogen: Pyruvate dehydrogenase E1 alpha. InsP_3R-1 antibody was provided by Dr. S. Joseph (Thomas Jefferson University, USA). Secondary antibodies conjugated with peroxidase were purchased from Amersham (Piscataway, NJ, USA).

Chemicals

Rapamycin, 3-methyladenine, dichloroacetic acid, methyl-pyruvate, doxycycline, ionomycin, FCCP, oligomycin, myxothiazol, rotenone, E-64d, bafilomycin A1, pepstatin A and Hanks' balanced salt solution were purchased from Sigma. Leucine free RPMI 1640 and DMEM were from U.S. Biological. L-690,330 and L-690,488 were from TOCRIS Biosciences. RU360, U73122, U73343, compound C and STO-609 were from Calbiochem. BAPTA-AM, BCECF-AM and propidium iodide (PI) were from Molecular Probes. Xestospongin B was extracted and purified from the marine sponge *Xestospongia exigua* as described (Jaimovich et al., 2005).

Cell Culture and Transfection

DT40 cells were maintained in suspension culture (Li et al., 2007). HEK293 Flp-In TRex cells (Invitrogen) stably expressing the tetracycline repressor and either an AMPK α1-K45R (dominant negative), AMPK α1-WT, AMPK shRNA or control shRNA (Hallows et al., 2009) were maintained and induced as described (Bhalla et al., 2006). HEK293-WT cells were maintained at 37°C (95%/5% air/CO_2) in DMEM media (GIBCO/BLR) supplemented with 10% (v/v) FBS, 100 U ml^{-1} penicillin, 100 μg ml^{-1} streptomycin. SH-SY5Y cells (American Type Culture Collection, Rockville, MD, USA) were maintained at 37°C (95%/5% air/CO_2) in a 1:1 mixture of Eagle's Minimum Essential Medium and F12 Medium, with 10% FBS. All cells were kept at low confluence to avoid autophagy induced by starvation. Transfections of DT40 cells were performed with a Nucleofector electroporator (Amaxa Biosystems).

Western Blotting and Treatments

Drugs were added in fresh media as indicated in text or figure legends. Treatments were terminated by rapid removal of medium with cells on ice, followed by cell lysis with Cytobuster protein extraction reagent (Novagen) supplemented with protease and phosphatase inhibitors (complete PhosSTOP, Roche). Protein extracts were separated in 4%, 10% or 15% SDS-polyacrylamide gels and transferred to PDVF membranes (Millipore). Blocking was at room temperature for 1 hr in 5% fat-free milk, and membranes were incubated overnight at 4°C with primary antibody, and then for 1 hr at room temperature with a secondary antibody conjugated to horseradish peroxidase. Chemiluminescence detection used ECL-plus reagent (Pierce) and a series of timed exposures of HyBlot CL film (Denville Scientific) to ensure densitometric analyses were performed at exposures within the linear range. To ensure equal protein loading across gels, membranes were submerged in stripping buffer (Restore western blot stripping buffer; Pierce), incubated at 37°C for 20 min, and re-probed with a loading control antibody. Films were scanned, and Image J was employed for densitometric analysis. Amount of LC3-II was normalized as LC3-I/(LC3-I+LC3-II), described as the most accurate quantitative method (Mizushima and Yoshimori, 2007).

Cell Viability

Viability assays were performed as described (Shimizu et al., 2004). Briefly, 3.5 × 10^6 cells were incubated in Hank's solution for 24 or 48 hr in the presence or absence of 10 μM 3MA. 2 μM propidium iodide (PI) was added to the medium and cells were observed under a fluorescence microscope (Nikon Eclipse TE2000). Over 1000 cells from 10 randomly selected fields were counted in each experiment.

Oxygen Consumption

Oxygen consumption rate (OCR) was measured in at 37°C using an XF24 extracellular analyzer (Seahorse Bioscience). Cells were seeded in 24-well plates treated with CELL-TAK (BD Bioscience). After 24 hr, cells were loaded into the machine for O_2 concentration determinations. Cells were sequentially exposed to oligomycin (1 μM), carbonylcyanide p-trifluoromethoxyphenylhydrazone (FCCP; 300 nM) and rotenone (100 nM) plus myzothiazol (100 nM). After each injection, OCR was measured for 5 min, the medium was mixed and again measured for 5 min. Representative traces shown in Figure 6A. Every point represents average of 10 different wells. Basal OCR was calculated as difference between OCR measured before and after oligomycin. Maximum OCR was calculated as difference between OCR measured after FCCP and that measured after exposure to rotenone plus myxothiazol. Data were normalized for protein concentration by lysing samples after each experiment.

In preliminary studies with each of the cell types, three concentrations of cells were seeded. Linear relationships between O_2 consumption and number of cells seeded were observed. We then chose the cell number that provided a nearly confluent uniform monolayer of cells. Before and again at the end of each experiment, uniformity of the monolayer was evaluated by DIC microscopy.

The integrity of the cells and the uniformity of the monolayer was again evaluated by DIC microscopy at the end of each experiment. Because DT40 lymphocytes normally grow in suspension, plates were pretreated with Cell-Tak to attach the cells.

Calcium Imaging

$[Ca^{2+}]_i$ was imaged using a total internal reflection (TIRF) microscope equipped with an Olympus X60 TIRFM objective (NA 1.45) (Smith et al., 2009). Fluorescence of cytosolic Fluo-4 was excited within the ~100 nm evanescent field formed by total internal reflection of a 488 nm laser beam incident through the objective at the coverglass/aqueous interface. Images of emitted fluorescence ($\lambda >$ 510 nm) were captured (128 × 128 pixels;1 pixel = 0.25 μm) at 100 frames s^{-1} (Cascade 128 EMCCD camera; Roper Scientific). Image processing and analysis were performed as described (Demuro and Parker, 2006). Fluorescence traces like those in Figure 7G were derived by measuring the average signal within 1.5 × 1.5 μm (6 × 6 pixel) regions of interest centered on Ca^{2+} release sites.

Atg5 KO Cells

Atg5 lox/lox mice (Hara et al., 2006) were infected with AAV-TGB-Cre or AAV-TGB-GFP (amplified and purified by the U. Pennsylvania Vector Core) for hepatocyte-specific expression of either Cre or GFP. Cells then were isolated by the two step perfusion method.

Lactate Measurements

Cellular lactate was measured by a colorometric assay kit (Abcam) according to the manufacturer's instructions.

Immunoprecipitation

Cells (HEK293 or DT40) were solubilized in 200 μl lysis buffer (20 mm Tris-HCl, pH 7.4, 0.1% Nonidet P-40, 1 mm EDTA, pH 8.0, EGTA, pH 7.8, 1 mm $Na_4P_2O_7$, 1 mm Na_3VO_4, 10% glycerol, 140 mm NaCl, 1 μg/ml aprotinin, 1 mm phenylmethylsulfonyl fluoride, and 1 μg/ml leupeptin). A 15,000 × *g* supernatant fraction was incubated with 10 μl A/G-Agarose beads (Santa Cruz, Biotechnology) for 30 min. The beads were pelleted by centrifugation and washed three times with washing buffer (25 mm HEPES, pH 7.5, 0.2% Nonidet P-40, 140 mm NaCl, 0.1% bovine serum albumin, and 10% glycerol). After the precleaning procedure, the whole-cell extract was incubated either with 1 μl of anti-$InsP_3R$-3 or anti-Beclin 1 for 1 hr and 50 μl of protein A-Sepharose (Santa Cruz Biotechnology). Immunoprecipitates were resolved by SDS-PAGE, transferred to polyvinylidene difluoride filters, and blotted with the corresponding antibody.

SUPPLEMENTAL REFERENCES

Hara, T., Nakamura, K., Matsui, M., Yamamoto, A., Nakahara, Y., Suzuki-Migishima, R., Yokoyama, M., Mishima, K., Saito, I., Okano, H., et al. (2006). Suppression of basal autophagy in neural cells causes neurodegenerative disease in mice. Nature *441*, 885–889.

Li, C., Wang, X., Vais, H., Thompson, C.B., Foskett, J.K., and White, C. (2007). Apoptosis regulation by Bcl-x_L modulation of mammalian inositol 1,4,5-trisphosphate receptor channel isoform gating. Proc. Natl. Acad. Sci. USA *104*, 12565–12570.

Mizushima, N., and Yoshimori, T. (2007). How to interpret LC3 immunoblotting. Autophagy *3*, 542–545.

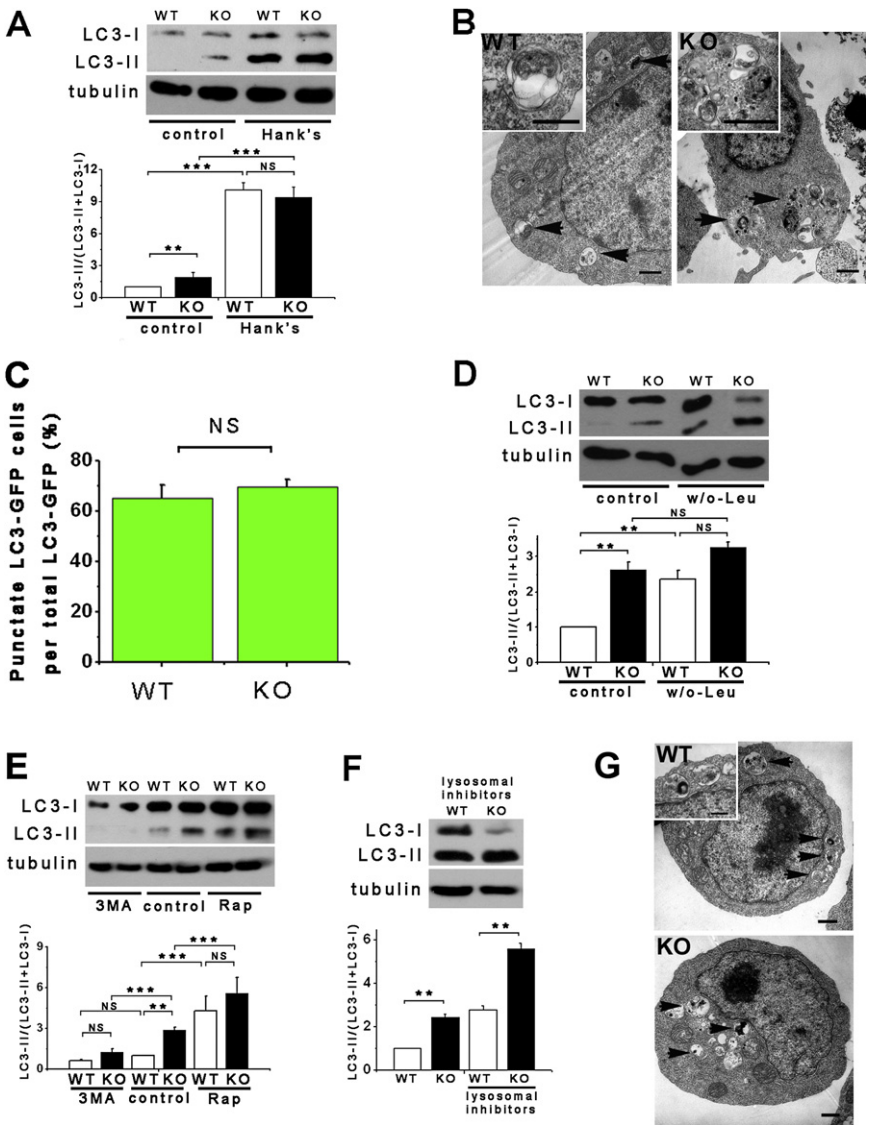

Figure S1. Nutrient Deprivation and mTOR Inhibition Induce Autophagy in Both DT40-WT and DT40-KO Cells, Related to Figure 1

(A) Nutrient starvation by incubation in Hank's solution for 12 hr induces autophagy in both DT40-KO and DT40-WT cells (n = 3).

(B) TEM of DT40-WT and DT40-KO cells after 12 hr starvation. Arrows and inset denote autophagosomes (AV). n = 3. Bars: 500 nm.

(C) GFP-LC3 puncta accumulation after 12 hr Hank's incubation. n = 3. (300 cells from 15 random fields per experiment). NS, not significant.

(D) DT40 cells were incubated in leucine free medium (w/o-Leu) for 1 hr. Graph represents LC3-II/(LC3-I + LC3-II) levels expressed as average fold increase (mean ± SEM, n = 3) over WT levels $^{**}p < 0.01$.

(E) Rapamycin (Rap, 10 μM) induces, and 3-methyladenine (3MA, 3 mM) represses autophagy in DT40-KO and DT40-WT cells. Cells exposed to treatments for 12 hr (n = 3).

(F) DT40 cells treated with lysosomal inhibitors pepstatin A (10 μg/ml) and E64D (10 μg/ml) and bafilomycin A1 (50 nM) for 12 hr. Graph represents LC3-II/(LC3-I + LC3-II) levels expressed as average fold increase (mean ± SE, n = 3) over WT levels $^{**}p < 0.01$.

(G) TEM of DT40-WT and DT40-KO cells after lysosomal function inhibition. Arrows show several AV in both cell lines. Bar, 500 nm.

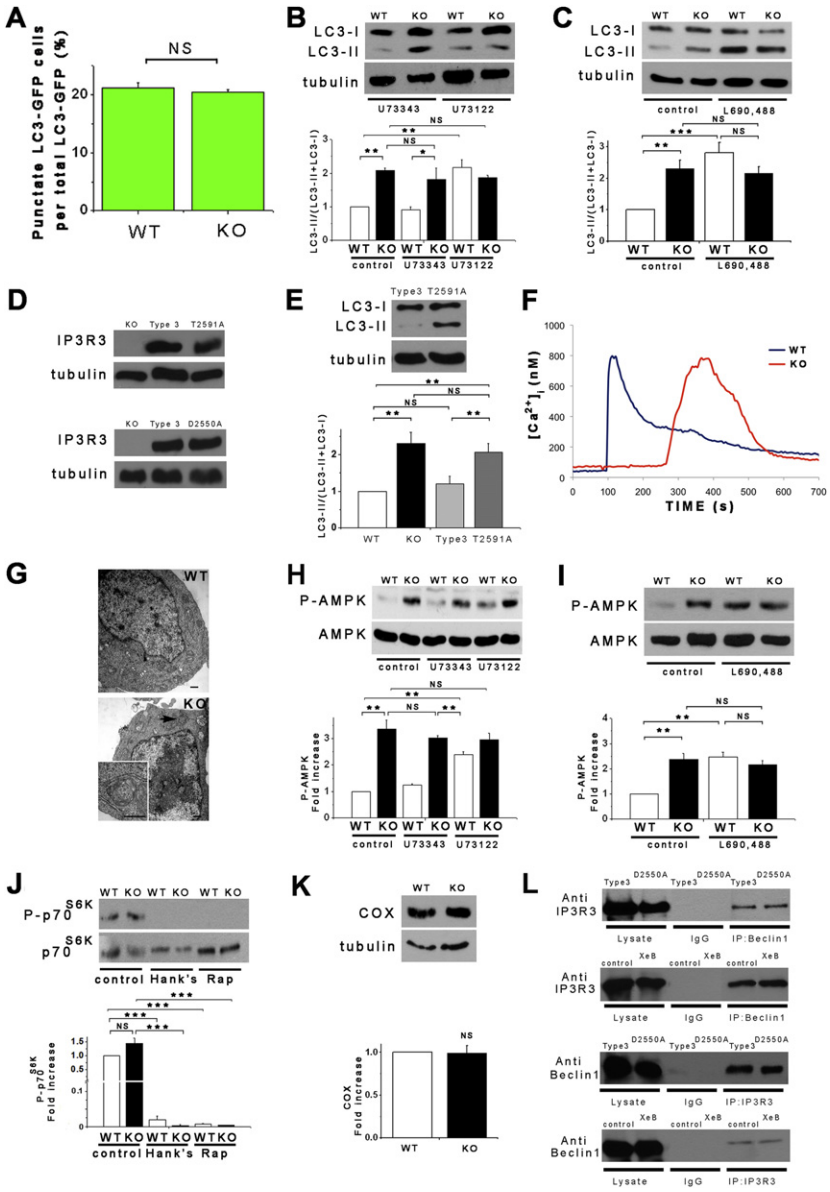

Figure S2. $InsP_3R$ Ca^{2+} Release Activity Specifically Is Required for Suppression of Autophagy and AMPK Activity, Related to Figure 2 and Figure 4

(A) GFP-LC3 puncta in DT40 cells treated with XeB (2 μM, 1 hr). n = 3 experiments (300 cells per experiment, 15 random fields per experiment).

(B and C) DT40-WT and DT40-KO cells treated either with phospholipase C inhibitor U73122, its inactive analog U73343 (both 5 μM, 30 min) or the inositol monophosphatase inhibitor L-690,488 (50 μM, 1 hr). Bottom graphs summarize results of six (B) or three (C) experiments.

(D) Expression of recombinant wt-$InsP_3R$-3, T2591A-$InsP_3R$-3 and D2550A-$InsP_3R$-3 in KO cells n = 3.

(E) Reintroduction of $InsP_3R$-3, but not a channel-dead T2591A-$InsP_3R$-3 suppresses autophagy in DT40-KO cells. Summary average fold increase (mean ± SEM) over WT cells n = 3.

(F) Representative traces of Ca^{2+} increases induced by caffeine (2 mM) in DT40-WT and DT40-KO cells stably transfected with RyR2.

(G) TEM of DT40-KO and DT40-WT cells stably transfected with RyR2. No presence of AV in KO cells (arrows, inset). Bar, 500 nm.

(H and I) PLC inhibitor U73122 (5 μM, 30 min) and inositol monophosphatase inhibitor L-690,488 (50 μM, 1 hr) trigger increase P-AMPK in DT40-WT cells, without affecting hyper-P-AMPK in KO cells. Inactive analog U73343 was without effect.

(J) Phosphorylation of mTOR substrates $p70^{S6K}$ in DT40 cells exposed to Hank's or rapamycin (Rap, 10 μM) for 1 hr. Levels expressed as average fold increase (mean ± SEM, n = 3) over basal levels.

(K) Expression of cytochrome c oxidase (COX) in DT40 cells. Summaries represent COX/tubulin levels expressed as average fold increase (mean ± SEM, n = 3) over WT or untreated basal levels.

(L) Coimmunoprecipitation of $InsP_3R$-3 and Beclin 1 was unaffected by the D2550A mutation in KO cells, or by XeB (2 μM) in HEK293 cells.

*p < 0.05, **p < 0.01; ***p < 0.001; NS, not significant.

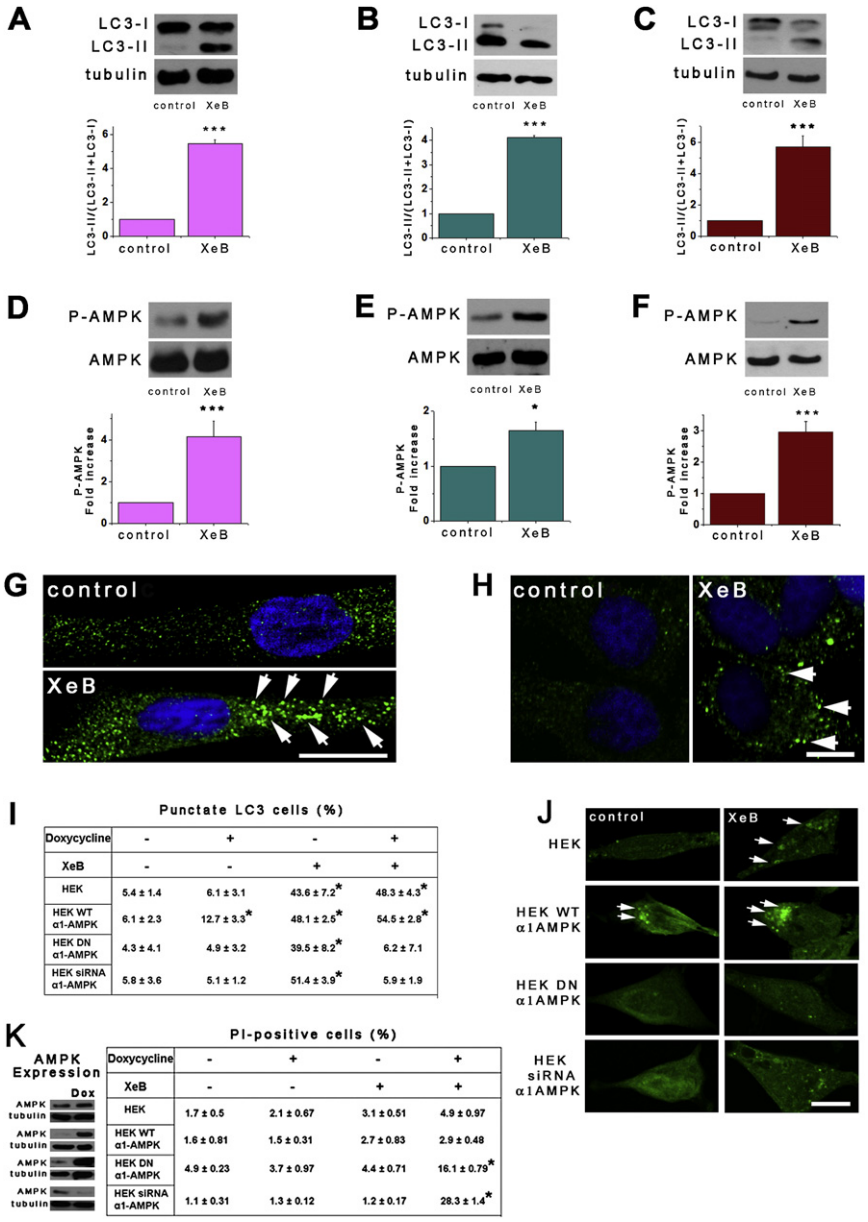

Figure S3. Inhibition of $InsP_3R$ Activity Activates AMPK and Autophagy in Multiple Cell Types, Related to Figure 2, Figure 4, and Figure 5

(A–C) Effects of XeB (2 μM, 1 hr) on autophagy marker LC3 or tubulin as loading control in MCF-7 (A), hepatocytes (B), and pulmonary smooth muscle cells (C). Summaries of LC3-II/(LC3-I + LC3-II) levels expressed as average fold increase (mean ± SEM, n = 3) over untreated conditions (autophagy basal levels).

(D–F) Effects of XeB (2 μM, 1 hr) on P-AMPK in MCF-7 (D), hepatocytes (E), and smooth muscle cells (F). Summaries represent mean ± SEM, n = 3. *$p < 0.05$, ***$p < 0.001$.

(G and H) Effects of XeB (2 μM, 1 hr) on LC3 pucta formation detected by immunolabeling in pulmonary smooth muscle (G), and MCF-7 (H) cells. Images representative of three different experiments. Arrows indicate autophagosomes. Bar: 10 μm.

(I and J) Effects of XeB (2 μM, 1 hr) on LC3 puncta formation detected by immunolabeling in Dox-treated HEK293 cells expressing Dox-inducible WT-, dominant negative (DN)- or siRNA-α1-AMPK. Images representative of three different experiments. Arrows indicate autophagosomes. Bar: 10 μm.

(K) Summary of effects of XeB on death (PI-positive cells) of HEK293 cells expressing doxycycline (Dox)-inducible WT-, dominant negative (DN)- or siRNA-α1-AMPK. Cells transfected with empty vector (EV) used as control (n = 3).

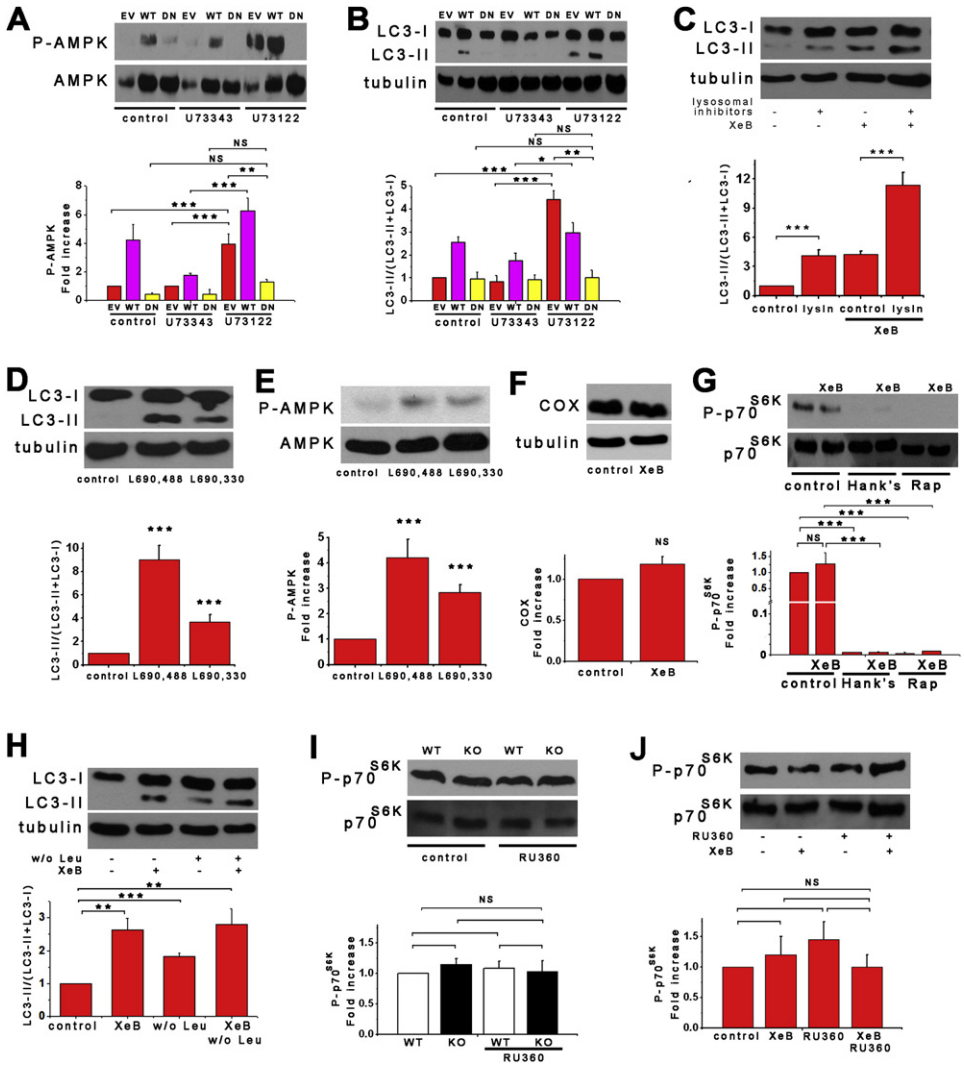

Figure S4. AMPK Activation Mediates mTor-Independent Autophagy Induced by Inhibition of $InsP_3R$, Related to Figure 5 and Figure 6

(A and B) Effect of PLC inhibition (U73122, 5 μM for 30 min) on P-AMPK (A) and autophagy (B) in HEK293 cells expressing induced-vector only (EV), wild-type AMPK (WT), or DN-AMPK (DN). Inactive U73343 was without effect. Graphs summarize six experiments (mean ± SEM).

(C) Effects of lysosomal inhibitors on autophagy in HEK293 cells. Cells treated pepstatin A (10 μg/ml), E64D (10 μg/ml) and bafilomycin A1 (50 nM) for 12 hr. Graph represents average fold increase (mean ± SEM, n = 3) over untreated cells.

(D and E) Effects on same HEK293 cells of inositol monophosphatase inhibitors L-690,488 (50 μM per 1h) or L-690,330 (100 μM, 1 hr) on autophagy (D) and P-AMPK (E). Graphs represent levels expressed as average fold increase (mean ± SEM, n = 3) over control cells.

(F) Expression cytochrome c oxidase (COX) in HEK293 cells. Summaries represent COX/tubulin levels expressed as average fold increase (mean ± SEM, n = 3) over WT or untreated basal levels.

(G) Phosphorylation of mTOR substrate $p70^{S6K}$ in DT40 cells exposed to Hank's or rapamycin (Rap, 10 μM) for 1 hr. Levels expressed as average fold increase (mean ± SEM, n = 3) over basal levels.

(H) HEK293 cells were incubated in a leucine free medium (w/o-Leu) for 1 hr and concomitantly treated with XeB (2 μM). Graph represents LC3-II/(LC3-I + LC3-II) levels expressed as average fold increase (mean ± SEM, n = 3) over untreated.

(I) Phosphorylation of mTOR substrates $p70^{S6K}$ in DT40 cells treated or not with 10 μM Ru360. Graphs represent levels expressed as average fold increase (mean ± SEM, n = 5) over basal levels.

(J) Phosphorylation of mTOR substrates $p70^{S6K}$ in HEK293 cells treated either with 10 μM Ru360, 2 μM XeB, or both together. Graphs summarize three experiments (mean ± SEM).

*p < 0.05, **p < 0.01, ***p < 0.001; NS, not significant.

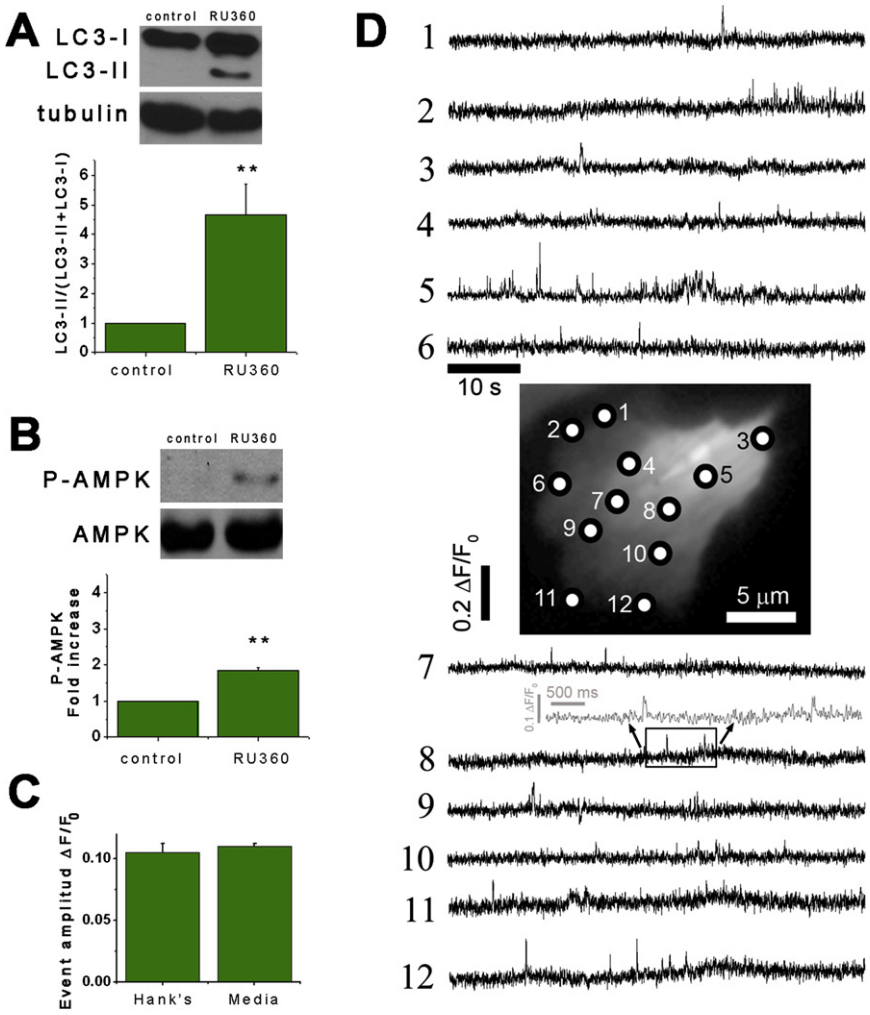

Figure S5. Spontaneous Local $InsP_3R$-Mediated Ca^{2+} Release to Mitochondria Suppresses AMPK and Autophagy, Related to Figure 7

(A and B) Effects of Ru360 (10 μM, 1 hr) on autophagy (A) and P-AMPK in SH-SY-Y5 cells (B). Graphs represent mean ± SEM of three different experiments. **p < 0.01.

(C) Summary fluo-4 peak event amplitudes in cells maintained either in Hank's or growth medium.

(D) Spontaneous local Ca^{2+} transients in SH-SY5Y cell bathed in culture medium. Image shows resting fluorescence of a single Fluo-4-loaded SH-SY5Y cell. Traces show fluorescence ratio signals ($\Delta F/F_0$) measured from each of the numbered regions of interest marked on the cell image. Grey trace shows segment of trace 8 outlined in the box at an expanded time scale.

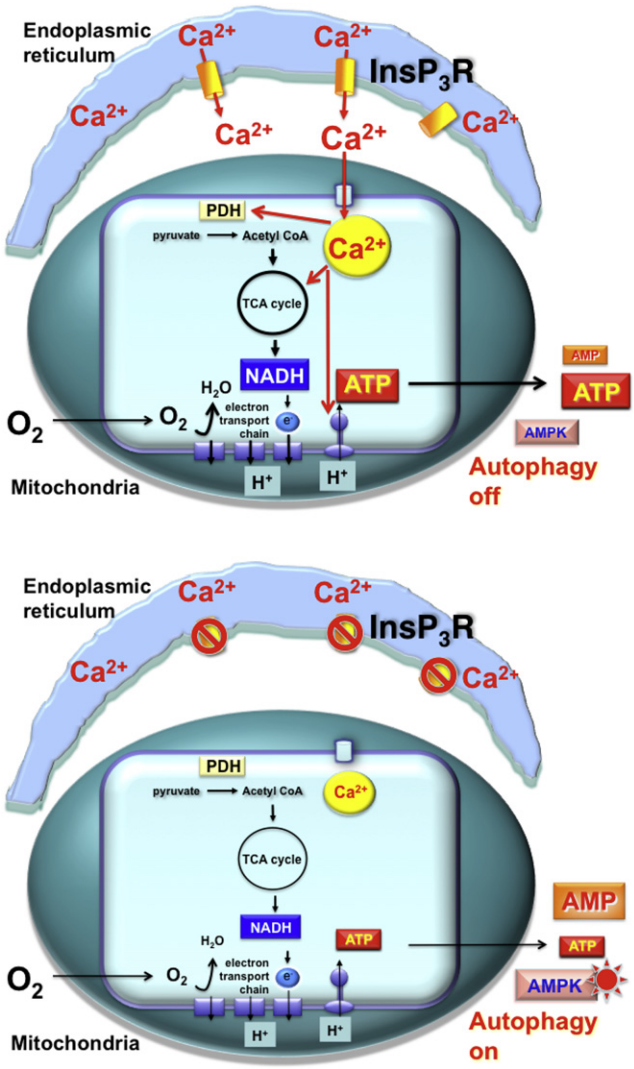

Figure S6. Mitochondrial Uptake of $InsP_3R$-Released Ca^{2+} Is Required for Basal Mitochondrial Bioenergetics, Related to Figure 7

Upper: Cartoon depicting constitutive delivery of Ca^{2+} from the endoplasmic reticulum (ER) to mitochondria, mediated by Ca^{2+} release through the $InsP_3R$ and mitochondrial uptake across the outer mitochondrial membrane by VDAC and the inner mitochondrial membrane by the Ca^{2+} uniporter. Matrix Ca^{2+} activates pathways, including pyruvate dehydrogenase (PDH) and dehydrogenases in the citric acid cycle, and the ATP synthase, that fuel the electron transport chain and O_2 consumption by providing reducing equivalents in the form of NADH. ATP production maintains a low cytoplasmic AMP:ATP ratio and bioenergetic fitness. Lower: In the absence of constitutive delivery of Ca^{2+} from ER to mitochondria, due either to genetic deletion of $InsP_3R$, inhibition of $InsP_3R$ activity (by xestospongin B (XeB) or inhibition of $InsP_3$ production [not shown]) or inhibition of mitochondrial Ca^{2+} uptake (Ru360), insufficient production of reducing equivalents (NADH) limits the activity of the electron transport chain, diminishing ATP production. Elevated AMP:ATP activates AMPK, which induces pro-survival, mTOR-independent autophagy.